11 Alternative and Specific Assessments for Fracture

11.1 Introduction

This section provides series of alternative and specific assessment routes to cover the special features of the case under consideration. There are numbers of special areas of the structural integrity assessment that need to be considered separately to provide detailed description of the case parameters to be used in the assessment. For example this section provides methodologies to cover the cases such as, leak before break, treatment of constraint, crack arrest, load history effect, mixed-mode, local approach, Charpy correlations, probabilistic and reliability, aerospace structures etc.

It is intended to provide additional information and detailed methodologies for selected cases to conduct assessment for better coverage of the structural case and hence reduce possible over conservatism if the assessment did not take into account of the special features described in this section.

11.2 Leak Before Break (LBB)

11.2.1 Introduction

There are several options by which it may be possible to demonstrate the safety of a structure containing flaws when an initial analysis has failed to show that adequate margins exist. For pressurised components one of these options is to make a leak-before-break case by demonstrating that a flaw will grow in such a way as to cause, in the first instance, a stable detectable leak of the pressure boundary rather than a sudden, disruptive break.

The various stages in the development of a leak-before-break argument may be explained with the aid of the diagram shown in Figure 11.1, [11.1]. This diagram has axes of flaw depth, a, and flaw length, $2c$, normalised to the pipe or vessel wall thickness, t. An initial part-through flaw is represented by a point on the diagram. The flaw may grow by fatigue, tearing or any other process until it reaches some critical depth at which the remaining ligament ahead of the flaw breaks through the wall. The flaw then continues growing in surface length until there is sufficient opening to cause a detectable leak or until the flaw becomes unstable. A leak-before-break argument is aimed at demonstrating that leakage of fluid through a flaw in the wall of a pipe or vessel can be detected prior to the flaw attaining conditions of instability at which rapid crack extension occurs.

This Section sets out procedures for making a leak-before-break case and recommends methods for carrying out each of the steps involved, including advice on the development of a part penetrating flaw. When applying the approach, it is important that additional calculations are carried out to assess the sensitivity of the results to likely variations in the input data. Guidance on this and other aspects of the analysis is given in Section 11.2.4 and it is important that this is read before using the procedures.

The starting point for the leak-before-break procedure is usually a surface flaw which has yet to break through the pipe or vessel wall. In order to make a leak-before-break case for this type of flaw, it is necessary to show that:

(i) The flaw penetrates the pressure boundary before it can lead to a disruptive failure;

(ii) The resulting through-wall flaw leaks at a sufficient rate to ensure its detection before it grows to the critical length at which disruptive failure occurs.

In the case of a through-wall flaw, (i) reduces simply to comparing the length of the flaw with the limiting length

Several steps are involved in establishing each of these requirements. First, the flaw must be characterised and the mechanisms by which it can grow identified. The next step is to calculate the length of the through-wall flaw formed as the initial flaw penetrates the pressure boundary; this is then compared with the critical length of a fully-penetrating flaw. Finally it is necessary to estimate the crack-opening area, the rate at which fluid leaks from the flaw, and whether or not the leak will be detected before the flaw grows to a critical length. These steps form the basis of the leak-before-break procedure described in Section 11.2.3 of this Section.

11.2.2 Scope

Where possible the leak-before-break procedures make use of methods and guidance already contained in other sections of this document. Where this is the case, for example, in the critical flaw size calculations, reference is made to the appropriate parts of the document. Methods other than those recommended in this procedure may be used but it is the responsibility of the user to ensure that the use of such methods can be justified and appropriate validation exists.

In contrast to the procedures of Section 6, which are concerned with failure avoidance, part of the leak-before-break case involves failure prediction. It is therefore recommended that best-estimate values of stresses and material properties, rather than pessimistic values, are used to estimate the flaw length at breakthrough when part-through flaws are being considered. However, to ensure conservatism, pessimistic values should be used to calculate the critical length of the resulting through-wall flaw, in accordance with the procedures of Section 6. For the purpose of this leak-before-break procedure the term 'limiting length' is used in this Section for the critical length of the through-wall flaw.

In assessing leakage, advice is offered which tends to underestimate flow rates as this is conservative. However, in some instances there may be consequences of leakage that have to be considered. In these cases an upper bound to leakage may be required, but this is outside of the scope of this Section.

Leak-before-break assessments for a pressure boundary should be conducted for locations judged to be most at risk. Some guidance on the selection of assessment sites is given in Table 11.1. The selection of assessment sites can be based on an elastic uncracked pipework system stress analysis, and the guidance given in Table 11.1. However, it may be necessary to examine several locations to ensure that the worst combinations of flaw orientation, loadings and material properties (eg. weld properties) have been accounted for. Although using stresses from an uncracked elastic pipework analysis may slightly underestimate the size of flaw to give a specified leak rate, several studies have shown that the conservatism associated with the determination of the limiting flaw length is overriding so that, overall, the use of uncracked-body stresses should be conservative in leak-before-break assessments [11.2].

The procedures are primarily aimed at the assessment of discrete flaws, either postulated or known to exist in a component, for which breakthrough would occur in a ductile manner. The procedures can in principle be used when the ligament beneath the flaw fails in a brittle manner but the re-characterisation rules following brittle ligament failure are such that it may not be possible to make a leak-before-break case without recourse to crack-arrest arguments.

A leak-before-break case may not be tenable in plant that is prone to cracking mechanisms that may lead to very long surface flaws. Also, the risk of transient water hammer loading in piping containing high energy fluid can preclude leak-before-break arguments, unless the peak loads can be adequately assessed and then considered in the limiting flaw size evaluation. Where there is significant risk of damage to piping from impacting (missiles or dropped loads), other whipping pipes or arising from equipment failure then such considerations should override any leak-before-break case.

11.2.3 Leak-Before-Break Procedure

The leak-before-break procedure is summarised in the form of a flow chart in Figure 11.2 and set out as a series of steps below. More detailed guidance on carrying out each of the steps is given in Section 11.2.4 the number in brackets after each step indicating the appropriate sub-section.

1. *Characterise the Flaw (Section 11.2.4.1)*

To use this procedure the flaw must be characterised as a surface (or through wall) flaw in accordance with Annex E. For extended, irregular flaws where a narrow ligament exists over only a small fraction of the overall flaw length the characterisation may be based on that part of the flaw where the narrow ligament exists. Embedded flaws must first be re-characterised as surface flaws in order to use the procedure.

2. *Determine Limiting Length, $2c_c$, of Through-Wall Flaw (Section 11.2.4.2)*

The limiting length at which a through-wall flaw at the position of the initial flaw would become unstable should be determined using the procedures contained in Section 6. The minimum limiting length should be determined for the most onerous loading condition using lower-bound values for materials properties. Where appropriate, stable tearing can be invoked in this part of the assessment.

3. *Estimate Flaw Length, $2c_b$, at Breakthrough (Section 11.2.4.3)*

The flaw length at breakthrough can be estimated using the procedures of Section 6 and the re-characterisation rules in Annex E. To determine the length at breakthrough:

(i) Assess the shape development of the characterised surface flaw (for example an inspection indication or postulated flaw) arising from potential crack growth mechanisms

(ii) Calculate the flaw length at which ligament failure is predicted to occur using the procedures in Section 6;

(iii) Re-characterise the flaw for which ligament failure is predicted to occur as a through-wall flaw using the rules of Annex E.

The flaw length at breakthrough, $2c_b$, is given by the length of the through-wall flaw resulting from (i)-(iii) above. Ligament failure should be assessed under normal operating conditions. Best estimates of material properties, loads and local collapse solutions should be used and ductile tearing should be taken into account. This provides a best estimate of the breakthrough length. The use of lower-bound material properties, lower-bound local collapse loads and a failure criterion based on initiation, reduces the breakthrough length and enhances the margin on flaw stability. The calculated leak rate is, however, reduced by this means. Because it is not clear which factor dominates, the use of best-estimate data is recommended. When assessing ligament failure, the front-surface length of the flaw, $2c$, should be compared with $2c_c$. If $2c > 2c_c$ prior to ligament failure, the flaw becomes unstable at the surface and a leak-before-break case cannot be made.

An alternative approach to calculating breakthrough length [11.3] avoids detailed ligament instability calculations. The initially part-through flaw is grown by fatigue or other sub-critical mechanism through the wall until the deepest point reaches the back surface. Since this neglects ligament instability, the flaw length at the initiating surface at breakthrough will be over-estimated. The stability of the surface point should be monitored throughout this process, as noted above. The flaw is then re-characterised as through-wall using the advice in Section 11.2.4.3.

4. *Calculate Crack-Opening Area of Flaw (Section 11.2.4.4)*

The crack opening area of the through-wall flaw is required to estimate leakage flow rates. The crack opening area depends on the flaw geometry (effective length, shape, orientation, etc.), the component geometry, the material properties and the loading conditions.

A best estimate approach to calculating crack opening area is advocated to establish the viability of a leak-before-break case, and provide a basis for the assessment of margins. However, crack opening area calculations are not simple and a bounding approach that minimises flow rates can offer alleviation of effort.

Advice on the calculation of crack opening area for idealised flaws in flat plates, pipework components and spheres is given in Section 11.2.4.4.

5. *Calculate Leak Rate from Flaw (Section 11.2.4.5)*

Computer codes are available to predict leakage rates for single and two-phase flows through a wide range of through-wall flaws. Details of these codes and approximate analytical solutions for isothermal and polytropic flow of gases are given in [11.4]. An alternative means of estimating the leakage rate is to use relevant experimental data if these are available.

6. *Estimate Time to Detect Leak from Flaw (Section 11.2.4.6)*

The leak detection system must be selected with due regard to the nature of the leaking fluid and the calculated leak rate. The detection time is then assessed from knowledge of the sensitivity of the equipment and its response time with due allowance for the need, if any, to check that the signal is not spurious.

The time for detection and the execution of the subsequently required actions must be less than that required for the flaw to go to the limiting length.

7. *Calculate Time to Grow to Limiting Length (Section 11.2.4.6)*

If the through-wall flaw can continue to grow in length as a result of fatigue or other mechanisms then the time required for the flaw to grow to a limiting length must be calculated by integrating the appropriate crack growth laws. Some fatigue crack growth laws are given in Section 7.

8. *Assess Results (Section 11.2.4.7)*

In principle, a leak-before-break case has been made provided that the calculations carried out in the preceding steps show that:

(i) the flaw length at breakthrough is less than the limiting length of a through-wall flaw;

(ii) the time to detect the leak is less than the time for the flaw to grow to a limiting length.

However, it is recommended that a sensitivity analysis be carried out to determine the extent to which changes in the input data affect the results of the calculations. Only if the above two conditions can be satisfied with adequate margins throughout the range of variations likely to occur in the input data can a satisfactory leak-before-break case be claimed. A sensitivity study can include failure based on initiation, with allowable tearing, and on instability. Also, upper bound material properties can be used, if known.

It should be noted that failure to demonstrate in the initial analysis that the flaw length at breakthrough is less than the limiting length, that the leak is detectable before the flaw grows to a limiting length, or that adequate margins exist does not necessarily mean a leak-before-break case cannot be made. As indicated in the flow chart of Figure 11.2, it may be possible to refine calculations, for example, by reducing any conservatisms that have been introduced into the calculations, by going to a more detailed analysis such as a finite element representation, or selecting a more sensitive leak detection system, and as a result make a satisfactory leak-before-break case.

11.2.4 Background Notes and Guidance on Using the Procedures

The following sections are intended to provide more detailed guidance on the methods recommended for carrying out the various steps in the leak-before-break procedure. It is recommended that these are read before using the procedure. Where it is relevant, background information on various aspects of the procedure is also included.

11.2.4.1 Flaw characterisation

The aim of flaw characterisation is to represent a known or postulated flaw by a relatively simple shape that adequately models the flaw and can be readily analysed. It is recommended that the flaw characterisation rules of Annex E are used for this purpose.

It is recognised that for extended, irregular flaws, where a narrow ligament may exist over only a small fraction of the overall flaw length, the characterisation rules of Annex E are likely to be unnecessarily pessimistic when making a leak-before-break case. For flaws of this nature it may be more realistic to base the initial characterisation on that part of the flaw where the narrow ligament exists. If this is done, however, it will be necessary to characterise and separately assess the remainder of the flaw to ensure that a critical part penetrating flaw cannot arise that would lead to a double edged guillotine break. Figure 11.3 illustrates such an example where a complex flaw has been separately characterised as the superposition of an extended, part-through flaw and a semi-elliptical flaw in a section of reduced thickness. Provided the extended flaw cannot grow to penetrate the wall before the semi-elliptical flaw breaks through, it is acceptable in this example to assess the leak-before-break behaviour of the complex flaw in terms of the behaviour of the more simple semi-elliptical flaw. If stable crack growth is to be invoked then provided that the flaw growth used in an analysis is compatible with the validity limits then the above re-characterisation is adequate.

If this approach is adopted, care will be needed in several areas to ensure that the leak-before-break case remains conservative. In reducing the section thickness, for example, the stresses in the remaining section must be increased to compensate for the loss of load-bearing area. Although this is conservative when calculating the limiting length of a through-wall flaw, the flaw length at breakthrough could be under-predicted as a result of the increased stresses. In this example it is therefore recommended that the breakthrough length is also calculated for a semi-elliptical flaw of length $2c'$ and depth $t-d$ having the same aspect ratio but based on the full section thickness; the larger of the two breakthrough lengths should be used in the subsequent calculations. In practice, L_r is unlikely to vary significantly and it may only be necessary to compare the K_r values at the deepest points of the two semi-ellipses to determine which has the greater length at breakthrough. Also, since the elastic COA is proportional to the applied stress and any flow reduction due to friction is proportional to the flow path length (and therefore the wall thickness), the COA and leak rate calculations should be based on a through-wall flaw in the full section thickness. This ensures that the predicted leakage remains conservative.

The flaw discussed above is just one example of a whole class of possible complex flaws which might require analysis. Other flaws may well need to be characterised in different ways in order to make satisfactory leak-before-break cases.

11.2.4.2 Calculation of limiting flaw lengths

As part of the leak-before-break procedures, the limiting length of a through-wall flaw at the position of the initial surface flaw must be calculated. It is recommended that this is done using the procedures of Section 6. It is important that the minimum limiting length is calculated for the most onerous loading condition, (this could be a frequent or seismic loadings case) using lower bound material properties relevant to the flaw location (eg. weld, parent or heat affected zone material). Where appropriate stable ductile tearing can be invoked within validity limits.

In determining the most onerous loading conditions, secondary stresses need to be considered using the procedures of Section 6, Annexes A and C.

11.2.4.3 Calculation of flaw length at breakthrough

Since the flaw length at breakthrough determines whether the initial failure results in a leak or a break it is important to correctly predict the shape of the flaw as it grows to penetration.

Ligament failure should be assessed using the stresses associated with normal operating conditions unless some other operating regime, prolonged operation at reduced pressure for example, leads to an increased flaw length at breakthrough. In calculating the breakthrough length it is assumed that ligament failure is not preceded by instability at the surface-breaking points of the flaw. However, the growth calculations may indicate that unstable growth in the length direction can occur before the flaw has grown fully through the wall. This result may be an artefact of the assumed flaw shape or of the use of limited ductile tearing. The methods of Section 6.4.3 may then enable the effects of the lower constraint at the surface point to be assessed. These aspects should be considered before concluding that a Leak-before-break case cannot be made. It is conservative for considerations of fracture to ignore ligament instability and to propagate the flaw through the wall by the appropriate sub-critical mechanism [11.3] as this will provide an over-estimate of the surface length at breakthrough. It should nevertheless be checked, by comparing the surface length with the limiting length $2c_c$, that instability at the surface points does not intervene.

To ensure that a leak can be detected, however, it is important that the flaw length and hence the COA at and following breakthrough are not over-predicted. It is recognised that when ligament failure first occurs, the flaw may not penetrate the wall along its entire length with a rectangular shape, as shown in Figure 11.4(a). It is also recognised that the flaw length at breakthrough, defined by the re-characterisation rules of Annex E, is itself likely to be an over-estimate of the actual length. Immediately following breakthrough, therefore, a cross-section of the flaw might appear as shown in Figure 11.4(b) for example. The initial leak rate may then be significantly less than that predicted on the assumption of a uniform flaw length equal to the flaw length at breakthrough as determined by ligament instability and flaw re-characterisation rules. In general this is not of concern since before the flaw can grow to a limiting length it will first grow to the breakthrough length, as determined by these rules. This argument is based on the assumption that if the flaw extends in length it tends towards a rectangular shape. The development of the shape of a flaw is illustrated in Figures 11.5 and 11.6, for surface and through-wall flaws, respectively. In some

cases, the stress distribution may be such that the flaw can increase in length whilst not tending towards a rectangular shape, but rather maintaining the shape at breakthrough, as shown in Figures 11.4(b) and 11.6(c), (d) without re-characterisation. The above argument no longer holds for such cases and estimates of COA based on a rectangular shape may be non-conservative unless based on the smaller of the surface lengths.

Recommendations are therefore given here for the flaw shape before, at and after breakthrough for cracked plates or cylinders subjected to either sub-critical fatigue/stress corrosion or ductile tearing situations. Figures 11.5 and 11.6 show the typical flaw shapes for sub-critical crack growth both during the surface crack growth (Fig. 11.5) and at and after wall penetration (Fig. 11.6). The recommendations are based on experimental and analytical studies [11.5] of cracked pipes and plates. Experimental data [11.6] for pipes under global bending lend qualitative support to Figures 11.5-6. In Figures 11.5 and 11.6 a distinction is made between initially 'short' flaws and 'long' flaws and also between predominantly tensile loading and through-wall bending. For mixed situations with both tensile and through-wall bending or moderately long initial flaws, interpolation between each case can be made. In general, it is assumed that the load levels are below yield so that plasticity effects should only have a small influence on the results. For fatigue crack growth, through-wall bending is assumed to correspond to an R-ratio close to zero. Note that the flaw shapes in Figure 11.5(c),(d) and Figure 11.6(c),(d) are for pure bending. For a small additional membrane stress component perpendicular to the flaw, the shape will behave more like the tensile-loaded cases (Figure 11.5(a), (b); Figure 11.6(a),(b)).

Growth of surface flaws

Table 11.2 summarises results [11.5] on the shape development of initially shallow surface flaws growing by sub-critical mechanisms.

Flaw shape at breakthrough

The back surface flaw length at wall penetration will be small [11.6-11.15], at least if the nominal stress is below yield. In addition, the front surface length at breakthrough will not be significantly different from that immediately before wall penetration. The following shape is recommended for the through-wall flaw immediately after breakthrough [11.5]:

$2c_1^*$ = surface crack length $2c_1$ just before wall penetration

$2c_2^*$ = min($2t, c_1/2$)

Here $2c_1$ and $2c_2$ are the front and back face flaw lengths, respectively and t is the wall thickness. The asterisk represents the conditions at wall penetration. Thus, the flaw shape at breakthrough is defined basically from the flaw shape immediately before wall penetration. The back face flaw length is set to a sufficiently small value which compares well with the reported fatigue experiments. This procedure is believed to work well if the load levels are sufficiently low to prevent significant ductile tearing after wall penetration. The back face flaw length at wall penetration is dependent on two parameters because for very long surface flaws, a back surface length $c_1/2$ would still be quite large, in conflict with experimental observations. On the other hand, for short surface flaws, e. g. a semicircular flaw, a back surface length equal to $2t$ will in general be larger than experimental observations.

Growth of the through-wall flaw

After wall penetration, the flaw shape again depends on the type of loading and the shape before wall penetration. Table 11.3 summarises results [11.5] on the shape development of sub-critical through-wall flaws after wall penetration. These start from deep surface flaws of different lengths just before breakthrough.

Flaw shape at breakthrough for ductile tearing situations

Figure 11.7 applies to the case where the loads during sub-critical growth are very large compared with yield, or if the cracked component is subjected to an increasingly high monotonic load such that growth by ductile tearing occurs.

Based on both numerical studies and experimental observations [11.6], the recommended back surface flaw length at wall penetration for high tensile loading is half the front surface length just before wall penetration (Figure 11.7(a)). In [11.5] it was observed from the finite element studies that the plastic zone size in the ligament in front of the deep surface flaw developed very quickly up to a distance corresponding to half the front surface length for each geometry considered. Furthermore, the J-integral values were quite high and uniform over this distance in the case of tensile loading. This advice (Figure I11.7(a)) was supported by ductile tearing experiments. For test SSTP12 [11.7], an increase of the load by 2% from that at wall penetration, increased the back surface flaw length to 90 mm (35% of the front surface length) at wall penetration. For a pipe test [11.16], immediately after breakthrough due to ductile tearing, the outer flaw angle reached 55% of the inner surface angle immediately before wall penetration.

The recommended back-surface flaw length at wall penetration for high through-wall bending is set to a distance equal to the plate thickness (Figure 11.7(b)). Very little experimental verification exists for this type of loading. However, numerical studies [11.5] where the J-integral values are suppressed at the deepest points of the surface flaw for plates subjected to high through-wall bending support a small back-surface flaw length at wall penetration.

For both types of loading, the front-surface flaw length at wall penetration is set equal to its length immediately before breakthrough plus the plate thickness. This allows for some ductile tearing also at the front surface at wall penetration and is supported by numerical results [11.5] and by a pipe test [11.16]. For simplicity, the recommendations in Figure 11.7 are valid irrespective of the initial aspect ratio of the flaw.

11.2.4.4 Calculation of crack-opening areas

COA models for plates, cylinders and spheres with through-wall flaws, and associated references, are summarised in Table 11.4. Estimates of COA can vary widely depending on how the flaw is idealised, which crack opening model is used and what material properties are assumed. This section provides advice on the factors which must be considered. Lower-bound COA solutions are set down for some simple geometries and loadings and references given to more detailed solutions. The advice will influence whether or not the simplified leak-before-break procedure where a through-wall flaw is assumed can be implemented. For example, the methods for calculating COA in the presence of weld residual stress fields will show the feasibility, or otherwise, of developing a detectable through-wall flaw at a weld location. Mean material properties should be used to provide a best estimate of COA. It is important to consider time-dependent changes in both material properties and loads, the latter arising from, for example, stress relaxation and stress redistribution processes. The plant loading conditions used for COA and leakage rate estimates are usually those associated with normal operation. If creep deformations at high temperature are being considered (Section 11.7), details of plant loading history may be required.

Estimation methods for COA can be classified into three categories: linear elastic models; elastic models incorporating a small-scale plasticity correction; and elastic-plastic models. Under load control and tensile through-wall stressing, plasticity leads to an increased COA compared with the elastic solution. Use of the elastic solution is then conservative in the leak detection element of a leak-before-break argument. Conversely, under displacement control, plasticity results in a reduction in COA.

A wide range of published solutions is available for idealised slot-like cracks in simple geometries subject to basic loads such as pressure, membrane and bending loads (Table 11.4). Their accuracy varies with the geometry and crack size, and with the type and magnitude of the load. Generally the models, except for results based on detailed finite element analysis, estimate the COA at the mid-thickness position; that is they do not account for crack taper, particularly that arising from through-wall bending loads. The effect of internal pressure is often represented by the equivalent membrane load. However, within the plastic range, the stress in the plane of the flaw can influence the COA and its effect should be considered [11.17,11.18]. For circumferentially-cracked cylinders in the absence of bending restraint, for example, the COA due to a tensile load is lower than that due to the equivalent pressure load and thus its use is conservative in a leak-before-break argument.

The COA can be calculated from explicit calculations of crack opening by integrating along the crack. Where results are given only for the crack opening displacement (COD), δ, at the crack centre, often an elliptical opening profile is assumed, so that the COA, $A = \pi c\delta / 2$. A diamond-shaped profile may be more appropriate for circumferential cracks of length greater than about half the pipe circumference, so that then $A = c\delta$ [I11.19, 11.20]. These simple relationships may not hold for asymmetric crack openings in complex geometries [11.21, 11.22]. Estimates of the COA for complex-shaped cracks, for example where a fully-circumferential flaw penetrates the pressure boundary along only part of its length, and for cracks at thickness transitions in pipes or at pipe-nozzle intersections, etc., may

be derived using more accurate models [11.22-11.26]. For such complex geometries and unusual crack configurations, or for calculations requiring a high level of confidence, it may be necessary to use the finite element approach to give accurate or even conservative COA results.

A lower-bound approximation to A, for a through-wall crack of length $2c$ in a shell with membrane stress σ_m and ratio, $S = \sigma_m / \bar{\sigma}$, of membrane to flow stress is [11.27]:

$$A = \alpha(\lambda) \frac{\pi \sigma_m c^2}{2E'} \left(\left(1 + \frac{S^2}{2} \right)^{3/2} - \left(\frac{S^2}{2} \right)^{3/2} \right) \tag{11.1}$$

The term in brackets represents a first-order correction for the effects of crack tip plasticity and increases with the loading level, S. The factor $\alpha(\lambda)$ is a correction to allow for bulging in terms of the shell parameter $\lambda = \left(0.75(1-\nu^2)\right)^{1/4} 2c / \left(Rt\right)^{1/2}$.

For axial flaws in cylinders with $\lambda \le 8$:

$$\alpha(\lambda) = 1 + 0.1\lambda + 0.16\lambda^2 \tag{11.2}$$

for circumferential flaws in cylinders with $\lambda \le 5$:

$$\alpha(\lambda) = (1 + 0.117\lambda^2)^{1/2} \tag{11.3}$$

and for meridional flaws in spheres with $\lambda \le 5$:

$$\alpha(\lambda) = 1 + 0.02\lambda + 0.22\lambda^2 \tag{11.4}$$

These expressions for $\alpha(\lambda)$ were derived using thin-wall, shallow-shell elasticity theory and are strictly valid only for mean radius to thickness ratios $R/t \ge 10$ and when crack lengths do not exceed the least radius of curvature of the shell. Alternative small-scale yielding models use explicit crack size corrections based on an effective crack length or angle [11.19, 11.20, 11.28].

Elastic finite element results for COA for cracks subject to combined primary and secondary stress in plates and cylinders and for through-wall self-balancing stress distributions enable the effect of these load types on COA to be assessed [11.29-11.31].

Background to and validation of the models in Table 11.4 for circumferentially-cracked cylinders is discussed in [11.32, 11.33]. For this geometry, more accurate elastic-plastic models have been formulated. These are recommended for best-estimate leak-befire-break calculations where stress levels are high enough to induce significant plasticity. Often, models require the stress-strain curve in Ramberg-Osgood form [11.28]. Reference stress methods, however, enable the material's stress-strain curve to be used directly [11.34]. Moreover, recent work enables the accuracy of reference stress estimates of COD to be improved by modifying the limit load [11.18-11.20, 11.35-11.40]. The modified limit load is defined as a geometry-, load- and crack size-dependent multiple of the conventional rigid-plastic limit load, and is calibrated using detailed finite element analyses. The multiplying factor is given for a range of crack angles and R/t ratios. Similar approximations for axially-cracked cylinders have also been obtained [11.41]. This approach enabled accurate prediction of COD for a large number of pipe test data.

The modified reference stress approach has also been formulated in terms of failure assessment diagram estimates of COD [11.38, 11.39]. The simplest approach requires only the material's yield and ultimate stresses. This was shown to conservatively under-estimate the COD compared with detailed finite element and experimental pipe test data for a range of pipe R/t values and loads. A second approach uses the full stress-strain curve and was shown to lead to more accurate and generally conservative results.

For bounding calculations of COA in cylinders, the linear elastic finite element results of [11.42] are recommended. These cover a wide range of cylinder geometries $(3 \le R/t \le 100)$ and flaw lengths. Elastic solutions, for the case of the circumferential flaw under axial tension, are also given in [11.19, 11.20] as explicit expressions for the factor α as a function of crack angle and R/t. The solution is extended to the case of global bending by multiplying the tension value of α by $(3+\cos\theta)/4$, where θ is the crack half-angle. The results agree well with those in [11.42].

Where elastic estimates of high accuracy are required it should be noted that non-linear geometric deformation effects can be important in some circumstances [11.43]. The solutions for plates and cylinders effectively assume that the flaws are in the centre of an infinite body. For many geometries this will be a reasonable approximation. However, if the flaw is close to a significant geometric constraint, for example a pipe-nozzle intersection, then local effects can influence the COA [11.21-11.26]. This is also true if significant through-wall bending stresses are present.

Most Leak-before-break assessments are likely to be concerned with the existence or potential existence of flaws at welds. The variation in material properties at welds, the influence of the weld preparation angle and the presence of residual welding stresses all affect the COA [11.22, 11.43,11.44]. A circumferential through-wall crack in a weld is analysed in [11.44]. For this situation the best estimate of COA is given by using the parent metal properties.

For pipework subjected to global transverse bending, the orientation of the resultant bending moment with respect to the through-wall crack must be considered [11.21, 11.46]. Off-centre loads can cause asymmetric and hence non elliptical crack opening or partial closure, or complete closure if the crack lies totally on the compressive side. Generally, finite element calculations have assumed a centred load.

For thick-walled geometries, the effect of crack-face pressure, which acts to open the flaw, will be a function of crack opening; for narrow cracks the mean pressure will be lower than for wide cracks. To assess the significance of such effects it is recommended that 50% of the difference between the internal and external pressures should be added to the membrane stress on the crack face. This value should then be re-assessed when undertaking the leakage flow calculations, which usually determine the exit pressure, and the results iterated if necessary.

Local through-wall bending stresses can induce elastic crack face rotations which reduce the effective COA. If complete crack closure occurs, no leak-before-break case can be made. Significant local through-wall bending stresses may be associated with weld residual stresses, geometric discontinuities, thermal gradients, or primary loads (for example hoop stresses in a pressurised thick cylinder). References for estimating elastic crack face rotations in simple geometries are included in Table 11.4.

The initial leakage rate through a flaw, which has just broken through the pressure boundary, may be significantly less than that predicted assuming a uniform flaw length equal to the re-characterised length (see discussion in Section 11.2.4.3 and Figure 11.4(b)). This is because when ligament failure first occurs, the flaw may not penetrate the wall along its entire length, and because the re-characterisation rules may over-estimate the actual flaw length. In general this is not of concern, since before the flaw can grow to a limiting length, it must first extend to the break-through length assumed in the COA calculations. However, for cases where through-wall bending stresses predominate, and development of a rectangular shape is unlikely (Figures 11.6(c), (d)), the COA can be minimised using the approximations in [11.47] by using a uniform lower-bound length based on the lesser of the two surface values.

11.2.4.5 Leak rate calculations

The calculation of the leak rate through a flaw is in general a complex problem involving the flaw geometry, the flow path length, friction effects and the thermodynamics of the flow. Several computer codes have been written to predict leak rates through cracks for a variety of fluids. Some of these are used in the recommended procedures for predicting leak rates outlined in this section. The codes are necessarily complex and have physical limitations as to their use; care should always be taken that they are used in situations for which they are valid.

For single-phase flow the following procedure for calculating leak rate is recommended, based on usage of the program DAFTCAT [11.48,11.49]. This program calculates flow rates for equivalent rectangular cracks and includes the effects of friction. The flow rate relation used is appropriate to isothermal or polytropic flow of gases:

$$Q = C_D (P\rho)^{1/2} WL \tag{11.5}$$

where Q is the mass flow through an equivalent rectangular flaw of mean width W and length L; P and ρ are the pressure and density, respectively, of the fluid at the crack entrance and C_D is the discharge coefficient, which includes the effects of friction.

DAFTCAT has been validated to some extent for artificial cracks [11.48, 11.50], with reasonable agreement observed between experiment and theory. Whilst measurements have also been made for real cracks [11.15, 11.16], the extent of validation is relatively small and the agreement with theory generally less good.

The derivation of the parameters required in Equation 11.5 is discussed in [11.4].

For two-phase flow of steam / water mixtures, a procedure based on the use of the program SQUIRT [11.51] is currently recommended. SQUIRT calculates critical two-phase flow rates for initially sub-cooled or saturated water flowing through cracks. A similar program, PICEP [11.52], which can also represent wet steam, is also recommended.

Both SQUIRT and PICEP have been validated by comparisons with flow through circular pipes, artificial and real cracks [11.50, 11.51]; reasonable agreement was observed between measurement and theory for artificial cracks. As with single-phase flow, the agreement between measurement and theory was variable in the case of real cracks. For cracks of width 50 μm or greater, calculated leak rates have been observed to differ from measured leak rates typically by a factor of 2 or less. However, for a crack of approximate width 20 μm, discrepancies of up to a factor of 9 have been observed. Commonly the discrepancy in leak rates for narrow cracks has been attributed to the effects of particulate plugging, though other factors such as uncertainties in crack dimensions may also be significant. These are discussed in [11.52].

Details of the thermal-hydraulic model of for the flow implemented in SQUIRT and the derivation of the model parameters are provided in [11.4].

11.2.4.6 Leak detection and flaw stability following breakthrough

Any leak-before-break procedure must show that the leaking flaw remains stable for a sufficient time to allow the leak to be detected. This time for detection should include that necessary to ensure that the signal is not spurious, or that to unambiguously identify the source of the leak and to take the subsequent required action. The stability of the leaking flaw needs to be assessed in terms of the margins to criticality and the potential for further crack growth. If further time-dependent crack growth can occur then margins on length and time to failure need to be demonstrated. The assessed time to failure, in conjunction with the estimated flow rate, permits a suitable leak detection system to be selected.

A wide range of leak detection systems is available. Some information and guidance on systems that are available is given in [11.54, 11.55]; here, only a brief outline is given here in terms of two broad categories: global and local. In the former category are leak detection systems that monitor large areas of plant or segregated regions. Examples include sump pumps, pumps for water systems, humidity detection for steam leaks, gas levels in air for gaseous systems, and radiation monitors for nuclear systems. All global systems detect all leaks (including, for example, valve glands, seals, etc), and hence any leakage identified by the monitoring equipment needs to be investigated and the source established. The response times for such systems are relatively long and depend on plant segregation.

Local leak detection systems monitor specific plant features (e.g. a weld) or a well-defined area (e.g. length of pipe). Some detectors are medium- or plant-specific. For example, moisture sensitive tapes only work in water or steam systems where condensation can take place on the outer surface.

Leakage through cracks generates acoustic emission that is transmitted through the structure, and, in some circumstances, through the air. Wave guide and microphone systems have been developed which offer flexible and sensitive leak detection capabilities for a wide range of fluids. Details of design and deployment depend on the application.

11.2.5 Assessment of Results

The final step in undertaking the recommended leak-before-break procedure is to carry out a sensitivity analysis. The sensitivity analysis must take into account the range of likelyvariations in the main parameters used in the calculations. It is particularly important to ensure that the sensitivity of the results to variations in material properties, applied loads and the predicted crack-opening areas and leak rates is investigated.

In carrying out the sensitivity analysis it is important to realise that, unlike the procedures in Section 6, where the use of upper-bound loads and stress-intensity factors together with lower-bound material properties and collapse solutions helps ensure that the integrity assessment is always conservative, a leak-before-break case made in this way would not necessarily be conservative. Although these bounding values provide conservative estimates of critical flaw length and are therefore recommended for the calculation of limiting lengths they minimise the flaw length at breakthrough and maximise the crack-opening displacement both of which are non-conservative when making a leak-before-break case. Best-estimate values should therefore be used to calculate the flaw length at breakthrough and crack-opening area and then the effect of varying input parameters examined.

When considering flaw stability at breakthrough, maximum conservatism is ensured by the use of lower bound material properties for the calculation of flaw growth in the surface direction, and the use of upper bound material properties for the calculation of through-thickness flaw growth and ligament instability. For conservatism in the prediction of crack-opening area, however, the reverse conditions could be adopted: the use of upper bound material properties for the calculation of flaw growth in the surface direction and the use of lower bound material properties for the calculation of through-thickness flaw growth and ligament instability. The sensitivity of results to methods used for the determination of flaw length at breakthrough (such as the use of local or global limit load solutions) should also be examined separately for stability and crack-opening area considerations.

Care should be taken to properly account for all loadings that may be imposed. Residual welding stresses and fit-up stresses, for example, are often not known to the same degree of precision as thermal, pressure and other operational stresses. It is important therefore that the sensitivity calculations reflect this uncertainty by allowing a suitably wide range of variation for these parameters.

The requirement to use best-estimate data should be borne in mind when choosing the analysis level. Where ductile tearing is likely to occur the use of such tearing provides more accurate estimates of limiting and breakthrough flaw lengths than an analysis based on initiation toughness. In practice the choice of level is likely to depend on other factors such as the availability of materials data. Nevertheless it is important from the point of view of assessing appropriate margins that any excessive conservatisms or possible non-conservatisms in the analysis are recognised and accounted for.

Prescribed margins are not advocated in this Section, and it is for the user to determine what margins are acceptable. It also needs to be recognised that what constitutes an adequate margin in one particular application may not be appropriate in another. Thus whether or not the margins demonstrated by the sensitivity analysis are deemed adequate is left to the judgement of the user. Although no direct guidance is given on quantifying what constitutes an adequate margin there are certain factors which should be taken into account when assessing the adequacy or otherwise of margins. These include the levels of confidence in the input data used in the calculations, any simplifying assumptions or approximations that may have been necessary, and whether or not the consequences of a sudden, break failure are tolerable.

When the procedure is used to assess discrete flaws, a possible result is that ligament failure may not be predicted under the prescribed loading conditions and neither a leak nor a break occurs. In such a case the sensitivity analysis should be used to determine the limiting conditions for ligament failure to occur and whether the failure would result in leak or a break.

11.2.6 Bibliography

[11.1] J K Sharples and A M Clayton, A leak-before-break assessment method for pressure vessels and some current unresolved issues, Int J Pres Ves Piping 43, 317-327 (1990).

[11.2] E Smith, The effect of system flexibility on the formulation of a leak before break case for cracked piping, Int Pressure Vessels and Piping Codes and Standards, PVP Vol 313-1, 129-135, ASME (1995).

[11.3] D G Hooton, Leak-before-break procedure for sodium boundary components, Design and Construction Rules Committee, Report No. 13, EFR B401 5 1465, Issue B, January (1993).

[11.4] R6: 'Assessment of the integrity of structures containing flaws', British Energy Generation Limited, Revision 4, June 2001

[11.5] B Brickstad and I Sattari-Far, Crack shape developments for LBB-applications, Engng Fract Mech 67, 625-646 (2000).

[11.6] Y S Yoo and K Ando, Circumferential inner fatigue crack growth and penetration behaviour in pipe subjected to a bending moment, Fatigue Fract Engng Mater Struct 23, 1-8 (2000).

[11.7] J K Sharples, The assessment of the results of AEA wide plate tests in terms of crack shape development following through-wall breakthrough, AEA Report AEA/RS/4453 (1994).

[11.8] J K Sharples, G Melvin, I J O'Donnell and S K Bate, Report of wide plate test SSTP13 to investigate leak-before-break of EFR Primary Vessel, AEA Report AEA/RS/4315, FR/SIWG/FESG/P(93)63 (1993).

[11.9] J K Sharples, L Gardner, D J Sanderson, G T Melvin and D Dobson, Report of wide plate test SSTP14 to investigate leak-before-break of EFR primary vessel, AEA Report AEA/RS/4361, FR/SIWG/FESG/P(93)68 (1993).

[11.10] K W Nam, K Ando, S Yuzuru and N Ogura, LBB conditions of plates and pipes under high fatigue stresses, Fatigue Fract Engng Mater Struct 15, 808-824 (1992).

[11.11] K W Nam, K Ando, N Ogura and K Matui, Fatigue life and penetration behaviour of a surface cracked plate under combined tension and bending, Fatigue Fract Engng Mater Struct 17, 873-882 (1994).

[11.12] K W Nam, S Fujibayashi, K Ando and N Ogura, The fatigue life and fatigue crack through thickness behaviour of a surface-cracked plate (effect of stress concentration), JSME Int J 31, 272-279 (1988).

[11.13] K W Nam, K Ando and N Ogura, The effect of specimen size on the behaviour of penetrating fatigue cracks, Fatigue Fract Engng Mater Struct 16, 767-779 (1993).

[11.14] Y S Yoo, S H Ahn and K Ando, Fatigue crack growth and penetration behaviour in pipe subjected to bending load, ASME Pressure Vessels and Piping Conference, San Diego, USA (1998).

[11.15] S H Ahn, A Hidaka and K Ando, Fatigue crack growth and penetration behavior in pipe subject to bending load, 14th Int Conf on Structural Mechanics in Reactor Technology, Lyon, France, 4, 113-120 (1997).

[11.16] D Moulin, S Chapuliot and B Drubay, Development of crack shape: LBB methodology for cracked pipes, LBB 95; Specialist meeting on Leak Before Break in Reactor Piping and Vessels, Lyon, France, October 1995; Proc US Nuclear Regulatory Commission, NUREG/CP-0155, 247-255 (1997).

[11.17] J Foxen and S Rahman, Elastic-plastic analysis of small cracks in tubes under internal pressure and bending, Nucl Engng Design 197, 75-87 (2000).

[11.18] Y-J Kim, N-S Huh and Y-J Kim, Quantification of pressure-induced hoop stress effect on fracture analysis of circumferential through-wall cracked pipes, Engng Fract Mech 69, 1249-1267 (2002).

[11.19] Y Takahashi, Evaluation of leak-before-break assessment methodology for pipes with a circumferential through-wall crack. Part III: estimation of crack opening area, Int J Pres Ves Piping 79, 525-536 (2002).

[11.20] Y Takahashi, Leak-before-break, Chapter 11, Volume 7, Comprehensive Structural Integrity, Elsevier (2003).

[11.21] N-S Huh, Y-J Kim, Y-J Kim, Y-J Yu and C-R Pyo, Effect of nozzle geometry on leak-before-break analysis of pressurised piping, Engng Fract Mech **68**, 1709-1722 (2001).

[11.22] S Rahman, N Ghadiali, G M Wilkowski, F Moberg and B Brickstad, Crack- opening-area analyses for circumferential through-wall cracks in pipes – part III; off-center cracks, restraint of bending, thickness transition and weld residual stress, Int J Pres Ves Piping **75**, 397-415 (1998).

[11.23] C C France, Crack opening area and stress intensity factor solutions obtained by finite elements for circumferential through-thickness cracks in cylinders under through wall bending - effect of modelled cylinder length and end restraints, AEA Technology Report SPD/D(95)400 (1995).

[11.24] R H Price, The effect of nozzle stiffness on the opening of a through wall crack in a spherical pressure vessel, Nuclear Electric Report TD/SEB/MEM/5015/92 (1992).

[11.25] Y-J Kim, N-S Huh and Y-J Kim, Crack opening analysis of complex cracked pipes, Int J Fract 111 71-86 (2001).

[11.26] Y J Yu, S H Park, G H Sohn, Y J Kim, and W Urko, Application of LBB to a nozzle-pipe interface, LBB 95; Specialist meeting on Leak Before Break in Reactor Piping and Vessels; Lyon, France, October 1995; Proc US Nuclear Regulatory Commission, NUREG/CP-0155, 81-89 (1997).

[11.27] C Wüthrich, Crack opening areas in pressure vessels and pipes, Engng Fract Mech 18, 1049-1057 (1983).

[11.28] S Rahman, F W Brust, N Ghadiali and G M Wilkowski, Crack-opening-area analyses for circumferential through-wall cracks in pipes – part I; analytical models, Int J Pres Ves Piping 75, 357-373 (1998).

[11.29] S F Yellowlees and A Toft, Elastic crack opening areas in thick-walled cylinders under primary and secondary loading, Serco Assurance Report SA/RD03123200/R01 (2002).

[11.30] M J Beesley and S F Yellowlees, Crack opening areas in plates under combined primary and secondary loading, AEA Technology Report AEAT/RJCB/000073/00 (2000).

[11.31] K Yahiaou, S F Yellowlees and C C France, Crack opening areas in plates under a self-balancing through thickness residual stress field, AEA Technology Report AEAT-6452 (2000).

[11.32] J K Sharples and P J Bouchard, Assessment of crack opening area for leak rates. LBB 95; Specialist meeting on Leak Before Break in Reactor Piping and Vessels; Lyon, France, October 1995; Proc US Nuclear Regulatory Commission, NUREG/CP-0155, 267-276 (1997).

[11.33] S Rahman, F W Brust, N Ghadiali and G M Wilkowski, Crack-opening-area analyses for circumferential through-wall cracks in pipes – part II; model validations, Int J Pres Ves Piping 75, 375-396 (1998).

[11.34] D B Langston, A reference stress approximation for determining crack opening displacements in leak-before-break calculations, Nuclear Electric Report TD/SID/REP/0112 (1991).

[11.35] Y-J Kim, N-S Huh and Y-J Kim, Enhanced reference stress-based J and crack opening displacement estimation method for leak-before-break analysis and comparison with GE/EPRI method, Fatigue Fract Engng Mater Struct 24, 243-254 (2001).

[11.36] Y-J Kim, N-S Huh and Y-J Kim, Effect of Lüders strain on engineering crack opening displacement estimations for leak-before-break analysis: finite element study, Fatigue Fract Engng Mater Struct 24, 617-623 (2001).

[11.37] Y-J Kim, N-S Huh and Y-J Kim, Reference stress based J and COD estimation for leak-before-break analysis of pressurised piping, Proc. ECF14, Krakow, II, 133-140 (2002).

[11.38] Y-J Kim and P J Budden, A reference stress based COD estimation in LBB analysis, Proc ECF13, San Sebastian , Elsevier (2000).

[11.39] Y-J Kim and P J Budden, Reference stress approximations for J and COD of circumferential through-wall cracked pipes, Int J Fract 116, 195-218 (2002).

[11.40] Y-J Kim, N-S Huh and Y-J Kim, Reference stress based elastic-plastic fracture analysis for circumferential through-wall cracked pipes under combined tension and bending, Engng Fract Mech 69, 367-388 (2002).

[11.41] Y-J Kim, N-S Huh, Y-J Park and Y-J Kim, Elastic-plastic J and COD estimates for axial through-wall cracked pipes, Int J Pres Ves Piping 79, 451-464 (2002).

[11.42] C C France, D Green and J K Sharples, New stress intensity factor and crack opening area solutions for through-wall cracks in pipes and cylinders, AEA Technology Report AEAT-0643 (1996); Addendum, April (1999). (See also ASME PVP, 350, 143-195, 1997.)

[11.43] J K Sharples and S Kemp, Effect of non-linear geometry on results of finite element calculated crack opening displacements in cylinders, AEA Report AEA/RS/4463 (1994).

[11.44] B R Ganta and D J Ayres, Analysis of cracked pipe weldments, EPRI Report NP-5057 (1987).

[11.45] P Dong, S Rahman, G Wilkowski, B Brickstad and M Bergman, Effects of weld residual stresses on crack-opening area analysis of pipes for LBB applications, LBB 95; Specialist meeting on Leak Before Break in Reactor Piping and Vessels; Lyon, France, October 1995; Proc US Nuclear Regulatory Commission, NUREG/CP-0155, 283-298 (1997).

[11.46] K A May, D J Sanderson and J B Wintle, Investigation of the effect of plasticity and non-centred bending on crack opening area for leak-before-break of piping systems, AEA Technology Report AEA-RS-4528 (1994).

[11.47] A P Hodgson and R H Leggatt, A review of the behaviour of penetrating fatigue cracks with reference to leak-before-break in the fast reactor. FRDCC/SIWG/DASG/P(87)156 (1987).

[11.48] A.F George, J I Rich, D H Mitchell and D J F Ewing, DAFTCAT - user guide, Nuclear Electric Report TD/SID/REP/0055 (1990).

[11.49] T C Chivers and D C Threlfall, DAFTCAT: New facilities and comparisons with ELF, Nuclear Electric Report EPD/REP/0008/96 (1996).

[11.50] C Chivers, The influence of surface roughness on fluid flow through cracks, Fatigue Fract Engng Mater Struct 25, 1095-1102 (2002).

[11.51] D D Paul, J Ahmad, P M Scott, L F Flanigan and G M Wilkowski, Evaluation and refinement of leak-rate estimate models: Topical Report, NUREG/CR-5128 Rev.1 (1994).

[11.52] D M Norris and B Chexal, PICEP: Pipe crack evaluation program (Revision 1), EPRI Report NP-3596-SR Revision 1 (1987).

[11.53] J Taggart, Leak before break – developments in leak-rate calculation methods for R6, Serco Assurance Report SA/SIS/14606300/R001 (2002).

[11.54] D H Mitchell, Leak detection systems in support of leak before break arguments, CEGB Report RD/B/6205/R89 (1989).

[11.55] T C Chivers, Aspects of leak detection, LBB 95; Specialist meeting on Leak Before Break in Reactor Piping and Vessels; Lyon, France, October 1995; Proc US Nuclear Regulatory Commission, NUREG/CP-0155, 485-489 (1997).

Consideration	Influence on LbB Arguments
Pipe Size	For given operating conditions and operating stresses, leak rates will be less for smaller pipes.
Stresses	For a given geometry, material and temperature, LbB margins tend to reduce as stress levels increase.
Components (elbows, tees, valves etc)	Likely to have complex stress fields which complicate LbB arguments and geometric stress raisers which can promote in-service degradation.
Welds and Castings	Flaws are more likely to occur in these features than in straight forged pipe made to modern standards.
Material Properties	Low yield stress, low fracture toughness and poor creep ductility make it more difficult to demonstrate a LbB case.
Susceptibility to degradation	Locations should be ranked against mechanisms such as fatigue, continuum damage, ageing, etc. Other mechanisms such as stress corrosion cracking, erosion, corrosion, etc may preclude a LbB case.
Leak Detection	The detection system used may have to change for different potential crack locations and leak rates.
Consequences	Acceptability of guillotine failure may determine which locations should be assessed.
Inspection	History or feasibility of future inspections may be a crucial factor in choosing locations for assessment.

Table 11.1 Guidance on selection of assessment sites around a pipe system.

	Tensile Load	Through-wall Bend
Short surface flaw	Figure 11.5a Growth in length and depth directions. Aspect ratio $2c/a$ effectively unchanged.	Figure 11.5c Growth in both directions, but much greater in length. Aspect ratio large as flaw approaches breakthrough.
Long surface flaw	Figure 11.5b Growth mainly in depth. Aspect ratio reduces.	Figure 11.5d Growth greatest at surface. Aspect ratio may decrease as flaw approaches breakthrough, depending on initial size. Final aspect ratio similar to Figure 11.5c.

Table 11.2 Advice on growth of surface flaws [11.4]

	Tensile Load	Through-wall Bend
Short through-wall flaw	Figure 11.6a Growth at both surfaces, but greater at back surface. Flaw tends to rectangular shape. In pure tensile load, difference between front and back surface lengths less than 10% when front surface 1.5 x breakthrough length. Rectangular shape reached after front surface length has grown to 2x front surface breakthrough length.	Figure 11.6c For initially deep flaw, growth much faster along front surface. Rectangular shape not reached. (If starter flaw is shallow, surface length grows to create long and deep flaw prior to breakthrough.)
Long through-wall flaw	Figure 11.6b Growth mainly at back surface until flaw near rectangular shape.	Figure 11.6d For initially long and deep surface flaw, growth along front surface faster than back surface, but less than Figure 11.6c. Small back surface length at breakthrough. As front surface length increases, back surface length increases but always lags behind.

Table 11.3 Advice on growth of through-wall flaws [11.4]

GEOMETRY	PRIMARY LOADING	ELASTIC OR SMALL-SCALE YIELDING		ELASTIC-PLASTIC
		ELASTIC MODEL	PLASTIC MODEL	
Plates	Membrane	Westergaard [III.11.54] Takahashi [III.11.26]	Wüthrich [III.11.33]	-
	Membrane + Through-Wall Bending	Miller [III.11.55]	-	-
Spheres	Membrane	Wüthrich [III.11.33] R/t > 10, $\lambda \leq 5$	Wüthrich [III.11.33]	-
	Membrane + Through-Wall Bending	Miller [III.11.55]	-	-
Cylinders with Axial Cracks	Tension	France et al. [III.11.48], $3 \leq R/t \leq 100$	Wüthrich [III.11.33]	Kim et al. [III.11.47]
	Through-Wall Bending	France et al. [III.11.48], $3 \leq R/t \leq 100$	-	-
Cylinders with Circumferential Cracks	Tension	France et al. [III.11.48] $3 \leq R/t \leq 100$ Takahashi [III.11.25-26]	Wüthrich [III.11.33] Rahman et al. [III.11.34]	Langston [III.11.40] Takahashi [III.11.25-26] Rahman et al. [III.11.34] Kim et al. [III.11.24, III.11.41-45]
	Global Bending	France et al. [III.11.48], $3 \leq R/t \leq 100$ Takahashi [III.11.25-26]	Wüthrich [III.11.33] Rahman et al. [III.11.34]	Langston [III.11.40] Takahashi [III.11.25-26] Rahman et al. [III.11.34] Kim et al. [III.11.24-26, III.11.41-45]
	Tension + Global Bending	Add elastic components	Wüthrich [III.11.33] Rahman et al. [III.11.34]	Takahashi [III.11.25-26] Rahman et al. [III.11.34] Kim et al. [III.11.24, III.11.44-46]
	Through-Wall Bending	France et al. [III.11.48] $3 \leq R/t \leq 100$	-	-

Table 11.4 Crack opening area methods for sinmple geometries and loading

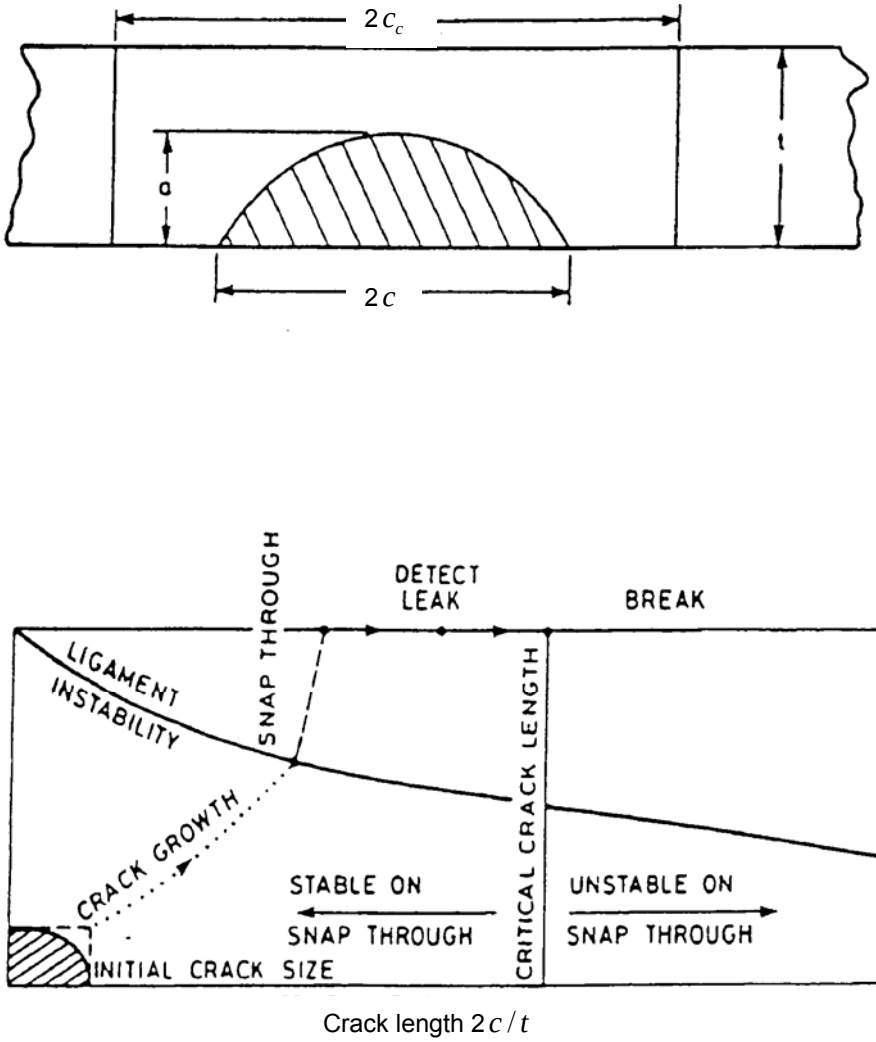

Figure 11.1 – The leak-before-break diagram

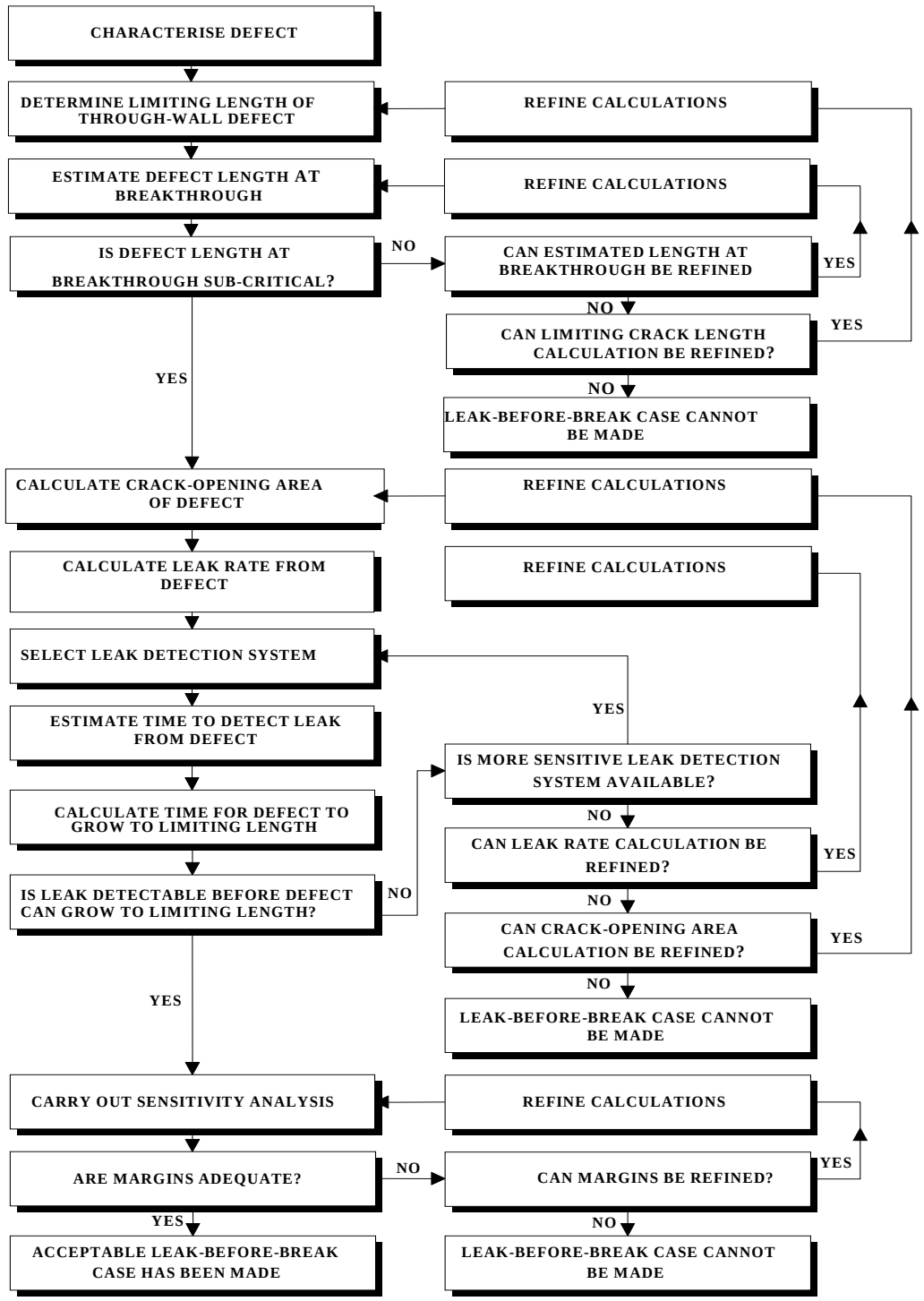

Figure 11.2 Flow Chart For Leak-Before Break

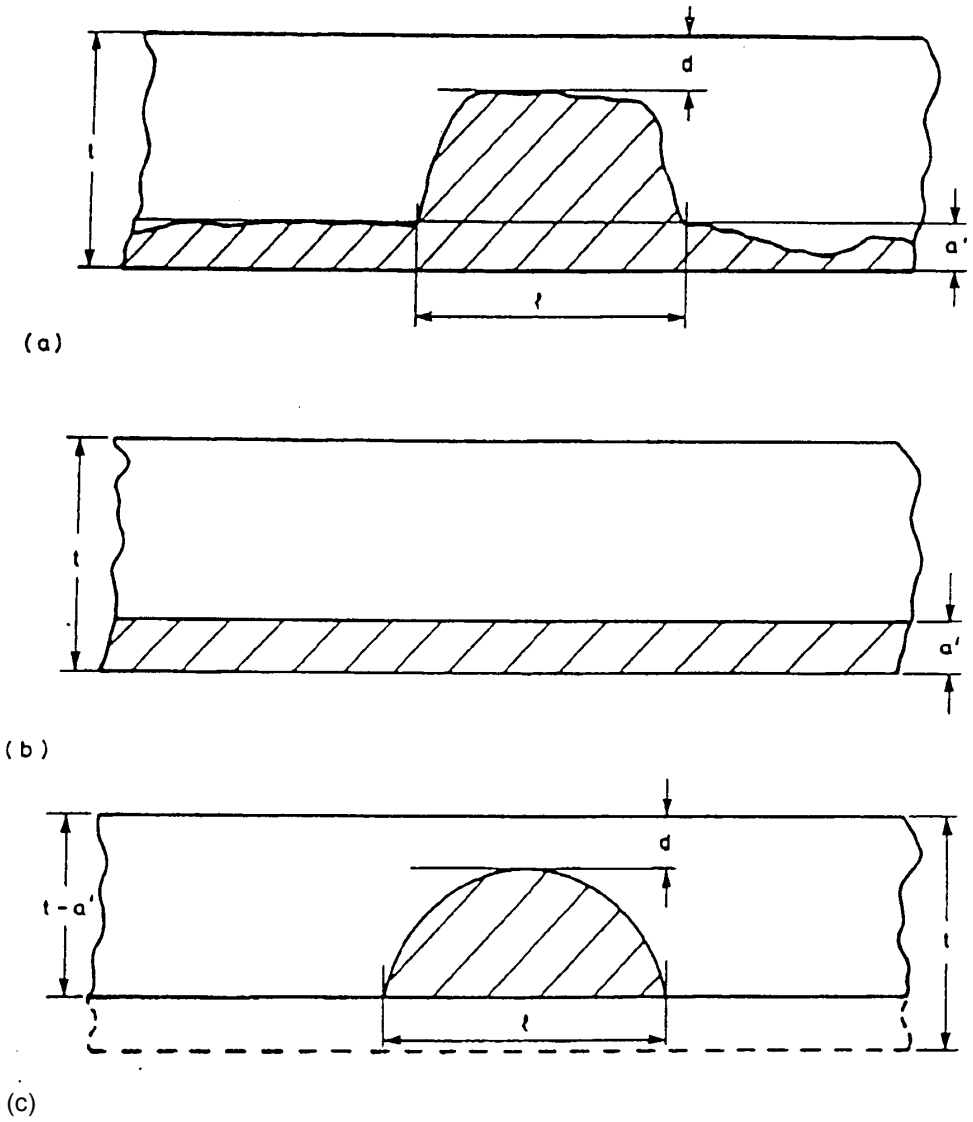

Figure 11.3 Example characterisation of a complex flaw. The complex flaw in (a) may be separately assessed as the two simple flaws in (b) and (c).

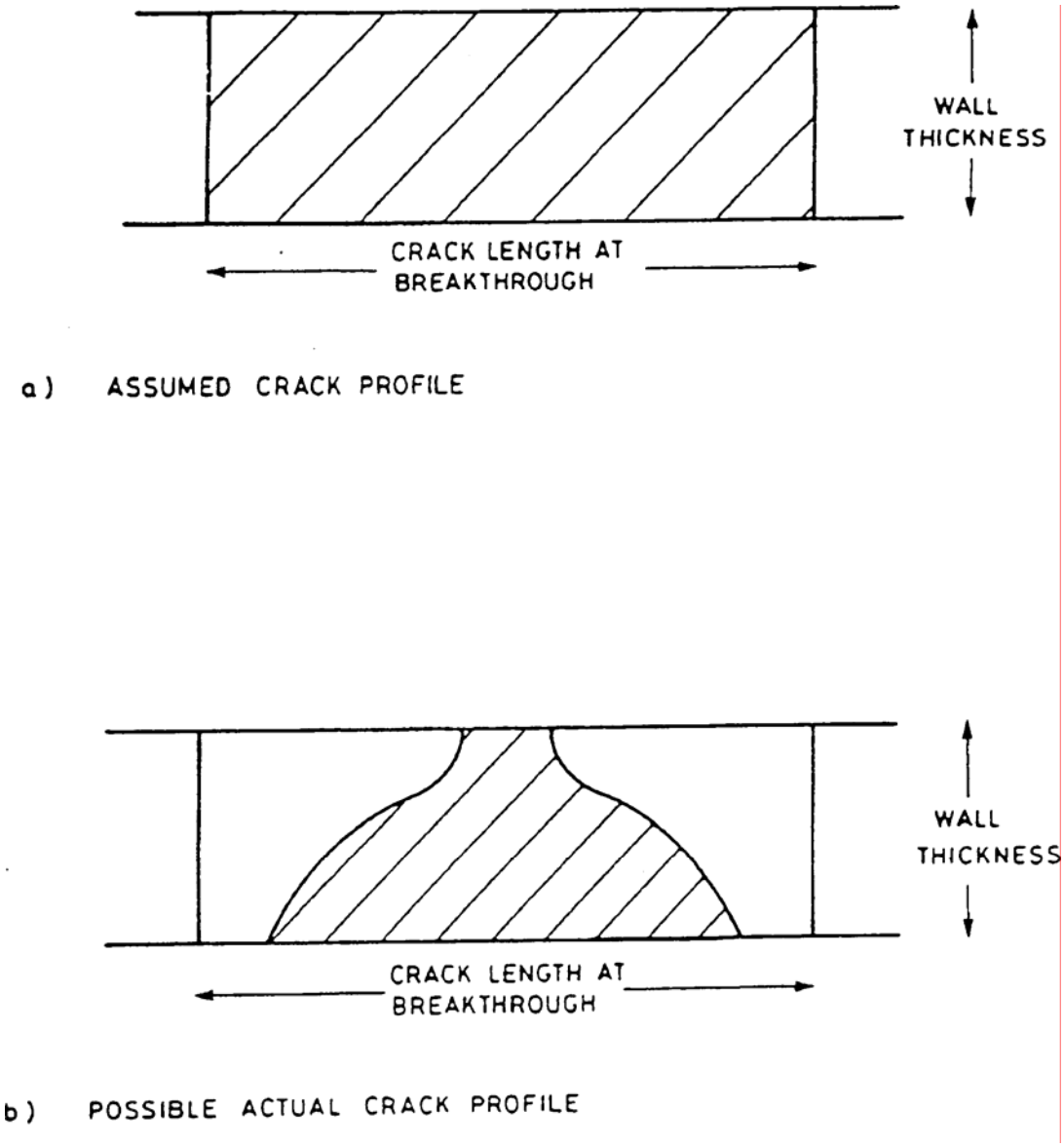

Figure 11.4 Schematic flaw profiles at breakthrough.

a) Tension, short crack

b) Tension, long crack

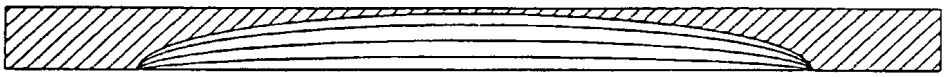

c) Bending, short crack

d) Bending, long crack

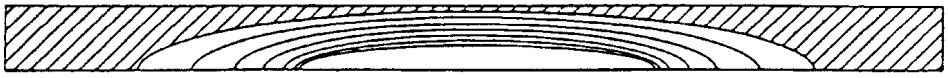

Figure 11.5 Development of flaw shapes for subcritical surface flaw growth.

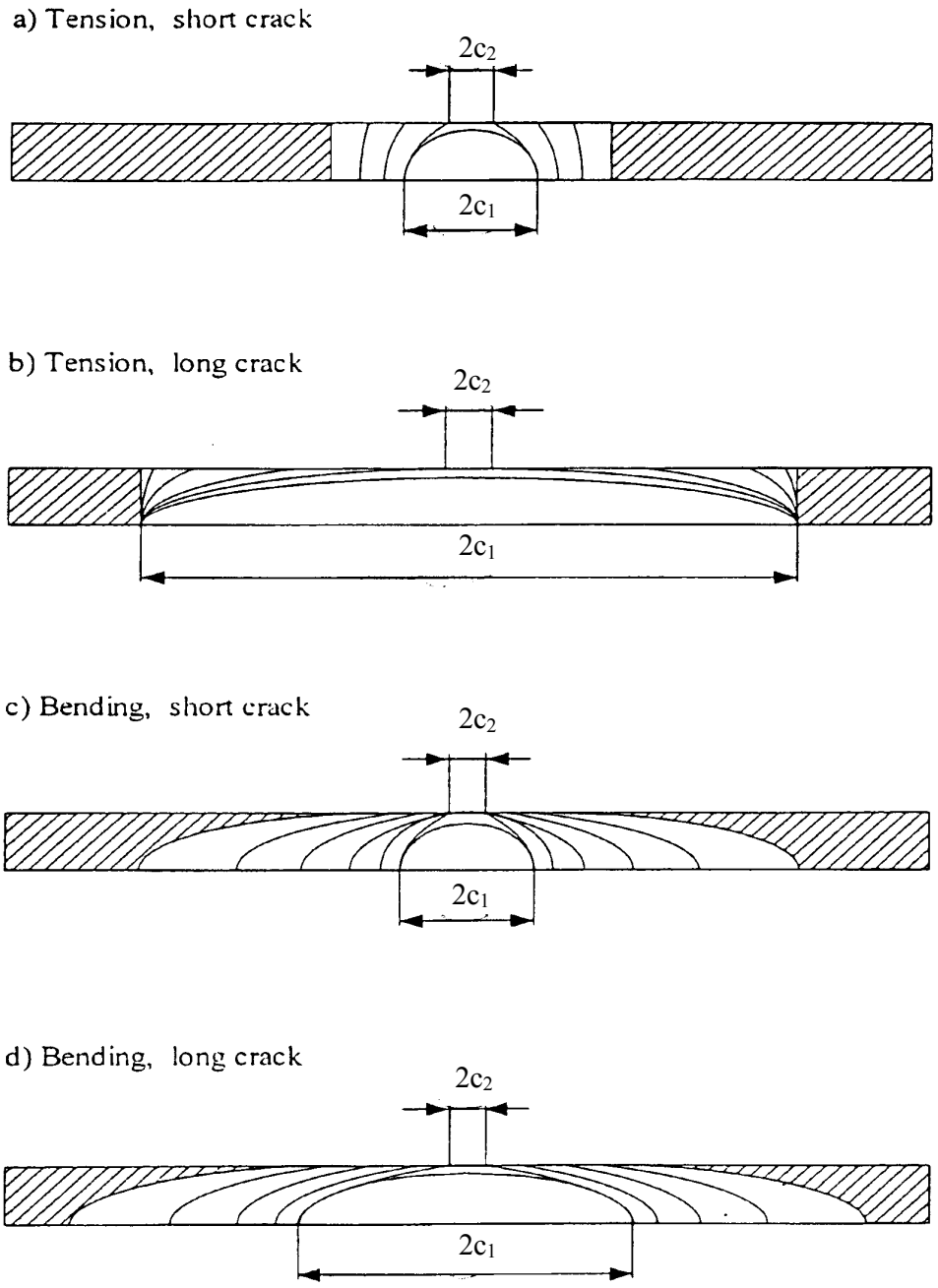

Figure 11.6 Development of flaw shapes for subcritical through-wall flaw growth.

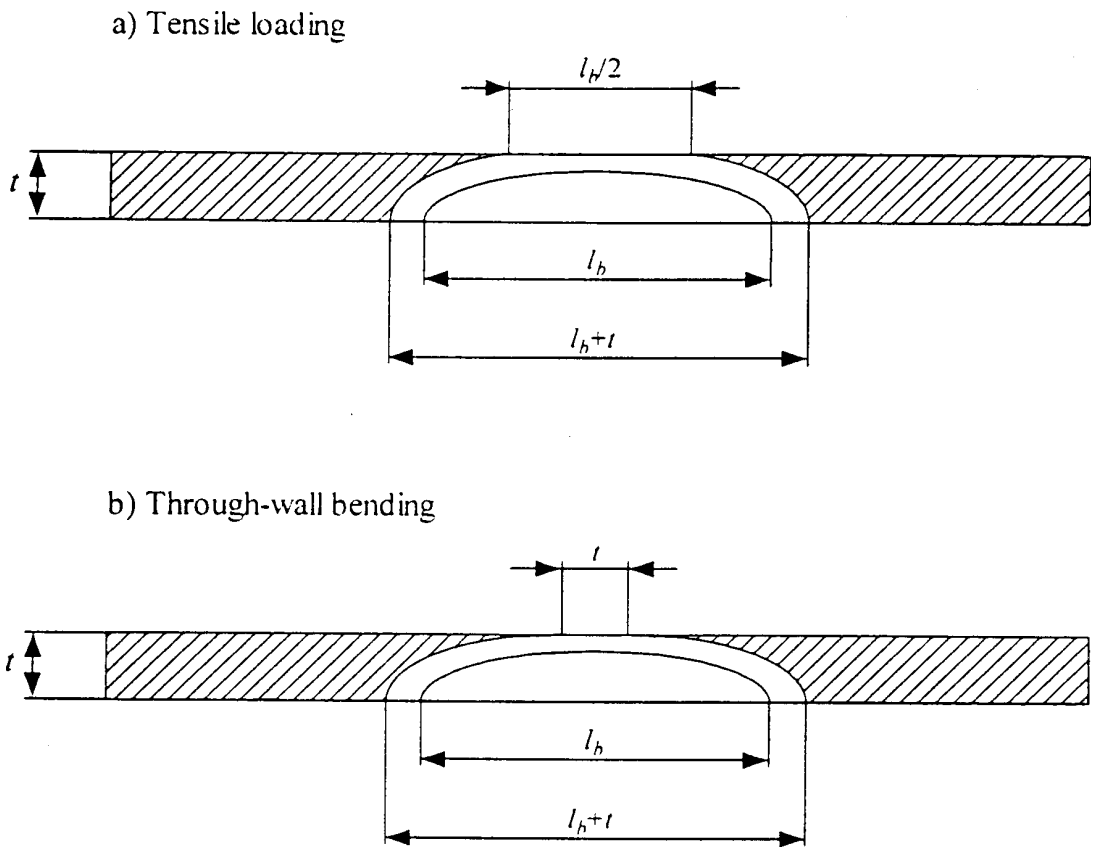

Figure 11.7 Recommended re-characterisation of flaws at breakthrough subjected to ductile tearing loading.

11.3 Crack arrest

11.3.1 Introduction

The procedure in Section 6 is based on the avoidance of failure by fracture or ductile instability. A complementary approach recognises the phenomena associated with the arrest of propagating brittle cracks, and evaluates limiting conditions in terms of fracture mechanics concepts involving crack arrest toughness or a related crack arrest temperature. The relationship between these two approaches is shown in Fig.11.8.

This section contains advice on the use of crack arrest in structural integrity analysis based on quasi-static approaches contained in R6 [11.56]. R6 also contains an approach based on dynamic analysis.

Following discussion of crack arrest phenomena in Section 11.3.2, examples of arrest are identified in Section 11.3.3. A procedure for assessing arrest is given in Section 11.3.4. Methods for the determination of the input quantities and advice on specific applications of arrest are given in Sections 11.3.5 - 11.3.7.

Section 11.3.8 give additional information on the evaluation of crack arrest material properties, and discusses some limitations of the methods presented. Much of the available advice is empirical [11.57], and the subject is undergoing rapid development. In particular, increased computational capabilities are enabling advances in the dynamic stress analysis of structures containing rapidly propagating cracks. These should facilitate development of advanced crack arrest approaches based on dynamic analysis.

11.3.2 Crack Arrest Phenomena

In [11.58, 11.59], a number of observations of crack arrest were used to identify the typical conditions for crack arrest. The structures were pressure vessels with a range of flaw types. Some had low toughness regions local to the flaw tip. In others, propagation and arrest of a fully penetrating flaw involved a considerable change of crack shape with an associated reduction in stress intensity factor. Crack arrest has also been observed during thermal shock tests on pressure vessels as a result of propagation from a cold region with low toughness to a warmer region with higher toughness.

Two conditions for crack arrest can be identified from these examples; these may occur separately, or in combination:

(1) the crack front enters a region of increased toughness;

(2) the stress intensity factor reduces as a result of propagation.

The application of crack arrest arguments requires material characterising properties to be quantified. Data are generally presented in terms of arrest toughness, K_{Ia}, or a crack arrest temperature (CAT). In the 1950s, CAT, derived from a mechanical testing procedure, was assumed to be a material constant. Now fracture mechanics describes rapid crack propagation and arrest by a relationship between dynamic crack tip driving force and dynamic fracture toughness. The dynamic toughness is dependent on temperature, so that although arrest can be expressed in terms of a CAT, the fracture mechanics approach suggests that CAT should not be regarded as a material property but as a function of other factors such as the level of applied crack driving force.

11.3.3 Scope

Figure 11. shows that structural integrity can in principle be guaranteed using arguments based upon either the avoidance of unstable fracture initiation, or the arrest of a propagating crack. Crack arrest assessment methods are less well developed than those for fracture initiation. Therefore, initiation-based arguments are generally used to demonstrate structural integrity, with crack arrest arguments providing a supporting role to give additional confidence.

The following examples have been identified as having the potential to lead to crack arrest, and for which the procedure of this section may be applied:

(1) crack propagation in a reducing stress gradient;

(2) crack propagation in a temperature gradient resulting from a thermal shock;

(3) crack propagation from an enclosed brittle zone;

(4) crack propagation in a region of varying toughness;

(5) crack propagation as a result of a load applied for a short duration.

The procedure of this section is limited to Mode I loading and to component response that is predominantly elastic. For mechanically loaded components, the criterion $L_r<1$ is sufficient to ensure this latter requirement. In principle, the procedure of Section 11.3.4 may be applied to other loading modes and at higher L_r values. However, in practice the required materials data are rarely available for other than Mode I loading.

11.3.4 Crack Arrest Assessment Procedure

Here, a quasi-static assessment procedure from [11.56] is presented. This requires a static stress analysis to provide the static stress intensity factor, K_I; this is multiplied by an enhancement factor, f_s, to allow for dynamic effects. The criterion for crack arrest is that the enhanced stress intensity factor should be lower than the static crack arrest toughness, K_{Ia}.

A dynamic assessment procedure is also presented in [11.56]. That approach describes the arrest of a crack in terms of dynamic fracture mechanics principles, and velocity or strain-rate dependent material properties. In principle, the dynamic procedure can provide a comprehensive analysis of crack arrest. However, it is not currently practicable to perform the materials tests to obtain velocity or strain-rate dependent arrest and dynamic toughness values, nor, for some engineering structures, the computation of dynamic stress intensity factors.

The steps in the quasi-static procedure are based on the flow chart shown in Figure 11..

(i) Define a postulated crack propagation path.

(ii) Define the assessment temperature, T_{op}, as the temperature in the neighbourhood of the tip of an arrested crack.

(iii) If data are available, determine the CAT, Section 11.3.7; if not proceed to step (v).

(iv) Arrest is predicted if CAT < T_{op}; if so, proceed to step (x).

(v) Define the loads externally applied to the structure, and also other conditions contributing to stresses in the region of the crack. Carry out a static structural stress analysis, distinguishing between primary stresses (σ^p) and secondary stresses (σ^s). Advice is given Section 5.3 on the categorisation of loads and stresses.

(vi) Determine the applied stress intensity factor (SIF) for a range of postulated arrested crack dimensions, including both σ^p and $\sigma^{s\,s}$ stresses.

(vii) Determine an enhancement factor, f_s, Section 11.3.5.

(viii) Determine the crack arrest toughness, K_{Ia}, for the assessment temperature, T_{op}, Section 11.3.7.

(ix) Arrest is predicted if f_s x SIF < K_{Ia}.

(x) Carry out an analysis of the arrested crack using the procedures of Section 6.

(xi) Perform a sensitivity analysis.

11.3.5 Determination of Enhancement Factor, f_s

The enhancement factor, f_s, can be obtained from an elastodynamic structural analysis. The peak dynamic stress intensity factor, $K_I^{dyn(peak)}$, immediately after arrest, and the static stress intensity factor, K_I, should be determined. The value of f_s is the ratio $K_I^{dyn(peak)}/K_I$. Consideration of the calculations and discussion in [11.60] suggests that f_s = 1.5 is a conservative estimate for application to structures.

The highest values of f_s are likely to occur when the value of the dynamic stress intensity factor is well below the current value of static stress intensity at the moment of arrest; for example, if a crack were travelling at high speed under increasing static stress intensity through a brittle zone. The recommended value of 1.5 is appropriate to this situation. Lower values of f_s, approximately 1.0, would be applicable to situations where the crack has arrested in a decreasing static stress intensity and increasing toughness field of the type which arises from a thermal transient.

The importance of the assumed f_s value in an assessment should be examined by sensitivity studies in which the value of f_s is varied in step (ix), and considering arrest at different crack lengths until no re-initiation is predicted even with the highest value of f_s.

11.3.6 Notes on Specific Applications

Further advice is given here for a number of specific applications.

11.3.6.1 Crack Propagating in a Temperature Gradient Resulting from a Thermal Shock

This case involves time dependence of stress and material properties, so additional steps are required in the assessment.

(i) Determine the temperature distribution in the structure as a function of time following a thermal shock.

(ii) Carry out stress analyses of the structure as a function of time, including the effect of the temperature distribution.

(iii) T_{op} is defined as the temperature in the neighbourhood of the crack tip at the time of the crack propagation event.

(iv) If arrest is predicted, re-assess the arrested crack for re-initiation of propagation at later times, noting the appropriate temperature distribution.

For this type of loading, there may be gradients of both applied stress intensity factor and crack arrest toughness with crack propagation distance. Confidence in an arrest assessment is increased when sensitivity studies demonstrate both that applied stress intensity factor reduces, and that crack arrest toughness increases, with postulated crack arrest distance.

11.3.6.2 Crack Propagation from an Enclosed Brittle Region

Some structures can be made of materials which have local regions of low crack initiation toughness. Failure avoidance may not be predicted for a small crack in such an enclosed brittle region using the low toughness in a

structural integrity assessment. There is the possibility that, if such a flaw were to propagate, it could arrest as the crack tip entered tougher material surrounding the brittle region.

The crack propagation path required in steps (i) and (ii) of the procedure may be difficult to predict. The user is advised to assume that the entire enclosed brittle region is fractured by a planar flaw defined by the maximum cross-section of the enclosed brittle region.

11.3.6.3 Crack Propagating in a Region of Varying Toughness

In Section 11.3.6.2, advice was given for materials with enclosed brittle regions. In other materials, toughness may be subject to a gradual variation with location throughout the structure. Arrest of a propagating crack is possible if the crack tip encounters sufficiently tough material. The crack arrest toughness and the crack initiation toughness should be defined as functions of position in the structure.

Arrest is predicted for a crack tip at a particular location if the enhanced stress intensity factor is below the corresponding toughness there.

Assessment should be carried out for a range of locations to provide a sensitivity study on flaw size to investigate the effect of the spatial distribution of toughness on arrest predictions. Confidence in an assessment depends on the crack size dependence of the margin between applied stress intensity factor and crack arrest toughness.

11.3.6.4 Short Duration Loads

A detailed stress analysis and assessment using the basic procedures should be carried out to determine whether a postulated crack would undergo crack initiation under the combination of any static load and the short duration load. Alternatively, crack initiation may be postulated.

Assume that the crack extends, increasing in size during the application of the short duration load in such a way that its maximum dimension is increased by the length $\Delta l = V_c \Delta t$, where V_c is the average velocity of the crack, and Δt is the duration of the load pulse. Current observations suggest an upper bound to V_c may be estimated as $V_{\tau/2}$ where V_τ is the velocity of transverse acoustic waves in the material assessed.

11.3.7 Determination of Toughness Values Used in Crack Arrest Assessment

The concept of toughness has been generalised to include a characteristic value of toughness at which crack arrest occurs in appropriate tests. In typical test specimens used to measure K_{Ia} crack propagation is induced at the root of a notch in the specimen, the shape of which is designed to provide a reducing stress intensity factor for a given load as the crack extends. Eventually the crack arrests, and the arrested crack length and the load determine a value of stress intensity factor, designated the crack arrest toughness. Similar analysis can be applied to larger structures, such as plates or vessels, in which crack arrest is observed, to provide estimates of toughnesses.

11.3.7.1 Static Crack Arrest Toughness, KIa

Static crack arrest toughness, K_{Ia}, is obtained through a static stress analysis of toughness specimens, or structures, in which crack arrest has been experimentally induced and observed. Details of a procedure, including validity limitations, can be found in [11.61]. Standard bend specimens may also be used. It is possible to interpret instrumented large-scale plate tests in terms of crack arrest toughness [11.62] by estimating stress intensity factors.

Indirect methods can be used to obtain K_{Ia} as a function of temperature.

For A533B-1, A508-2 and A508-3 steels, ASME [11.63] defines a lower bound function which was fitted to a range of toughness data, including crack arrest toughness. It relates toughness to temperature via a material dependent reference temperature, denoted RT_{NDT}, defined as the highest of the following:

(i) the NDTT from drop weight tests,

(ii) 33°C lower than the 68J Charpy temperature,

(iii) 33°C lower than the temperature at which a Charpy specimen achieves a lateral expansion of 0.89mm.

The lower bound toughness reference function is:

$$K_{IR} = 1.344 \exp[0.0261(T - RT_{NDT} + 88.9)] + 29.4\ MPa\sqrt{m} \quad (11.6)$$

with T and RT_{NDT} in degrees Centigrade. This function is used in an ASME procedure for determining the acceptability of flaws that have been detected during in service inspection [11.63]. Part of the procedure includes analysis for crack arrest based on static linear elastic fracture mechanics and equation (11.6).

An alternative approach based on predicting the mean value of K_{Ia} at a given temperature has been proposed by Wallin [11.64]. For a range of ferritic steels, the mean crack arrest toughness is described by:

$$\mathrm{K_{Ia}} = 30 + 70 \exp[0.019(\mathrm{T} - \mathrm{T_o})]\ \mathrm{MPa}\sqrt{\mathrm{m}} \quad (11.7)$$

where T_o is the temperature corresponding to $\mathrm{K_{Ia}} = 100\ \mathrm{MPa}\sqrt{\mathrm{m}}$. There is evidence that T_o is linearly correlated with NDTT, and also with T_{41J} and T_{Fa4}. Here, T_{41J} is the temperature for 41 Joules absorbed energy in a standard Charpy test, and T_{Fa4} is the temperature corresponding to a force of 4kN at brittle crack arrest measured on an instrumented Charpy specimen [11.65].

Whereas equation (11.6) is a lower bound expression, equation (11.7) is a best-estimate fit to data. In applications, the user should consider the possibility and significance of scatter of toughness values about the best estimate using a sensitivity study, and it is recommended to use a lower bound value for K_{Ia} in assessments.

11.3.7.2 CAT Determination

The CAT can be derived from the Robertson plate test [11.66]. A crack is induced by impact to propagate in the edge of a full thickness plate of the test material held under a tensile load representative of the required loading condition. Depending on the material temperature, the crack either continues to propagate and the plate fractures, or it arrests. The CAT is the critical temperature distinguishing these behaviours. The Esso test, which is similar to the Robertson plate test but has a larger gauge length, and the double tension test, in which crack propagation is initiated in a secondary loading tab welded to the main plate, by means of a subsidiary loading system, are described in [11.57]. The double tension test is a more recent development having greater controllability. Some large-scale crack arrest tests are isothermal, whereas others have a temperature gradient to promote arrest. Isothermal tests are preferable for defining CAT.

The various tests can be categorised as either large or small scale. The former have the full thickness of the test structure, and a potential crack propagation path of many times the thickness (eg Robertson, Esso and double tension tests). The remaining tests are small scale, and therefore cheaper and more convenient to perform, and are used to characterise aspects of material behaviour; they can provide a measure of a characteristic temperature, TT_{ss}, which is correlated with the CAT, and which is typically easier to obtain. It is found that, for a given range of steels, a relationship of the following general type can be obtained:

$$CAT = \alpha TT_{ss} + \beta \quad (11.8)$$

where α is a constant, approximately equal to unity, TT_{ss} is a transition temperature based on a small-scale test ([11.57] contains many examples), and β is an additional constant temperature.

For example, for C and C-Mn steels made in the 1960s, Nichols [11.67] found that CAT could be correlated with the 50% FATT derived from Charpy specimens, with $\alpha = 0.84$ and $\beta = 3°C$. For modern steels, a better correlation is obtained with $\alpha = 1$ and $\beta = 35°C$.

The conclusion in [11.68] is that the best correlations of CAT with small-scale tests occur with NDTT data obtained in Pellini drop weight tests. The CAT determined in plate tests is dependent on applied stress, σ, in MPa, and plate thickness, B, in metres:

$$CAT\left(°C\right) = NDTT + 21.7\ln\sigma + 173.2\left(200B - 1\right)^{1/13} - 285 \qquad (11.9)$$

Equation (11.9) is a best estimate correlation for plate thicknesses in the range 0.005m to 0.025m; an additional 15°C can be added to the value of CAT given by equation (11.9) to provide an upper bound when this is required in assessments.

11.3.8 Additional Information

Brittle crack propagation takes place at high speeds and involves high strain rates, and continued propagation can be regarded as governed by the balance between dynamic crack driving force and dynamic fracture toughness. The toughness is dependent on the fracture micro-mechanisms occurring under the pertaining local stress level and strain rate. At present, there is no standardised method for investigating dynamic fracture toughness.

With the quasi-static analysis procedure given here, dynamic re-initiation of a momentarily arrested crack necessitates the use of the enhancement factor, f_s, to relate the peak dynamic stress intensity factor, $K_I^{dyn(peak)}$, to the static arrest toughness. It is preferable if the value of f_s can be obtained for the specific structure being assessed by elastodynamic computation.

The CAT, when measured using full-thickness plate tests, was regarded as a material property. Subsequent measurements showed that CAT depends on the plate thickness, the applied stress level, and also the amount of energy stored in the system. Nevertheless, at temperatures above CAT brittle crack propagation leading to fracture does not normally occur when CAT has been measured in structurally significant tests. These are tests on plates with the full thickness of the structure and loaded to a stress level greater than or equal to the stress in service, in which arrest of a crack longer than the one to be assessed occurred before the interference of reflected stress waves. Crack arrest can also occur at temperatures below the CAT when the stress distribution in the structure is favourable.

Failure of specimens or structures above CAT can occur due to ductile processes. Examples are fracture toughness tests above the ductile to brittle transition temperature, drop weight tear tests and Charpy impact specimens, and the failure of pressurised pipes [11.69]. In each case, the load is maintained at a high enough level to allow ductile crack propagation and instability. Assessment for ductile failure should therefore always accompany a crack arrest assessment. It is expected that, in principle, the concept of arrest toughness can be generalised to include rapid ductile crack propagation. The same procedure would then apply to the arrest of ductile crack propagation, but crack arrest arguments cannot provide protection when ductile instability is predicted.

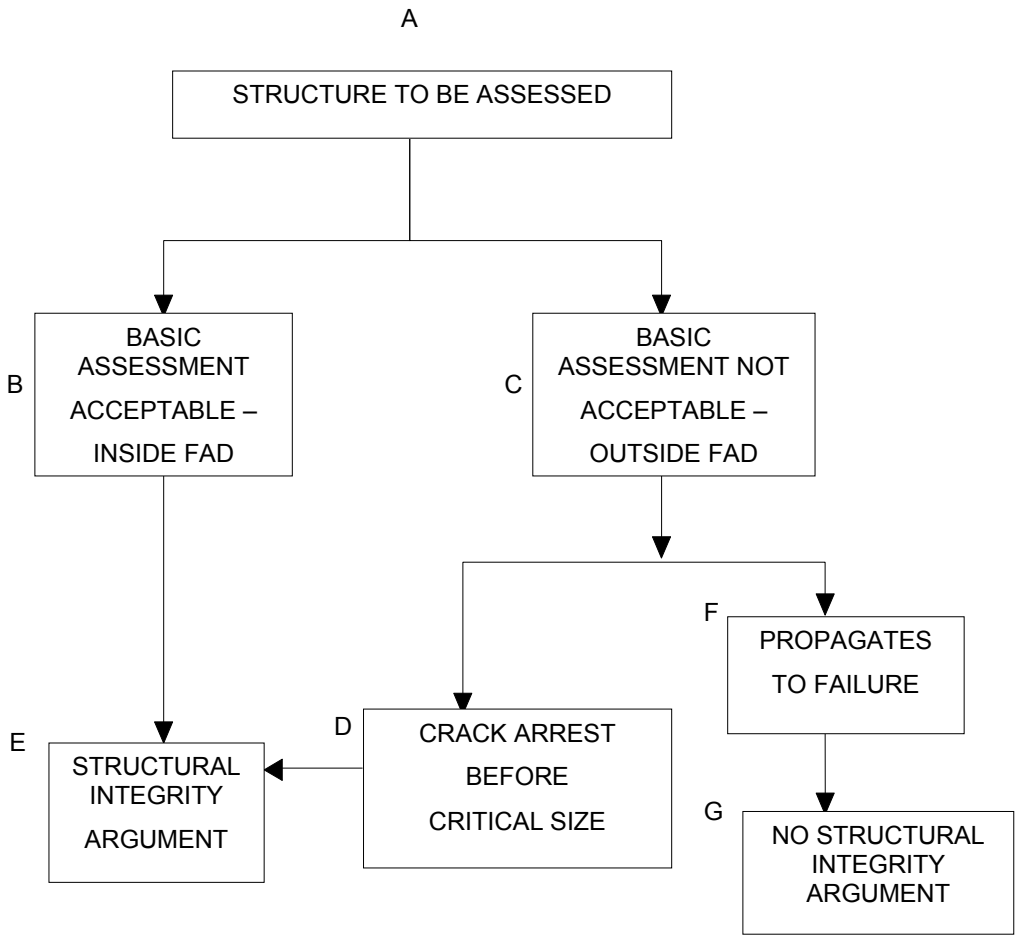

A, B, E	CURRENT BASIC APPROACH
A, C, D,E	CRACK ARREST APPROACH
A, C, F, G	NO STRUCTURAL INTEGRITY ARGUMENT

Figure 11.8 – Relationship between basic and crack arrest structural integrity assessment methodologies

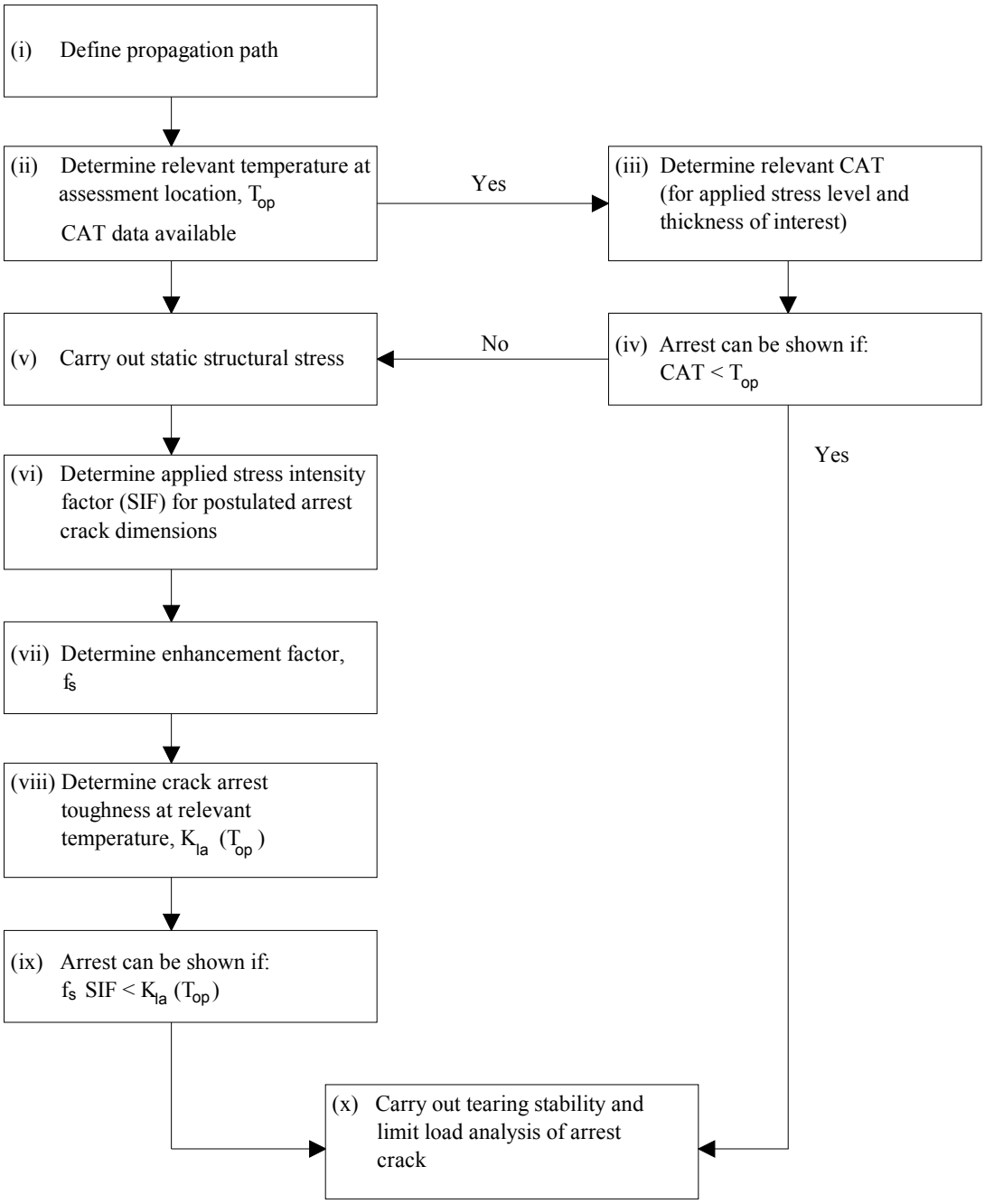

Figure 11.9 – Flow chart for crack arrest assessment procedure

11.3.9 Bibliography

[11.56] R6, Assessment of the Integrity of Structures Containing Flaws, British Energy Procedure (2000).

[11.57] C S Wiesner and B Hayes, A review of crack arrest tests, models and applications, Conference on crack arrest concepts for failure prevention and life extension, Abington, Cambridge (1995).

[11.58] F M Burdekin, J F Knott, J D G Sumpter and A H Sherry, TAGSI views on aspects of crack arrest philosophies for pressure vessels with thicknesses up to 100mm, Int J Pres Ves Piping **76**, 879-883 (1999).

[11.59] D C Connors, A R Dowling and P E J Flewitt, The relevance of crack arrest phenomena for pressure vessel structural integrity assessment, Conference on crack arrest concepts for failure prevention and life extension, Abington, Cambridge (1995).

[11.60] J D G Sumpter and R M Carr, Crack arrest concepts for structural safety justification, Conference on crack arrest concepts for failure prevention and life extension, Abington, Cambridge (1995).

[11.61] ASTM Standard E 1221-88, Standard test method for determining plane-strain crack-arrest fracture toughness, K_{Ia}, of ferritic steels, American Society for Testing and Materials (1988).

[11.62] C S Wiesner, B Hayes, S D Smith and A A Willoughby, Investigations into the mechanics of crack arrest in large plates of 1.5% Ni TMCP steel, Fatigue Fract Engng Mater Struct **17**, 221-223 (1994).

[11.63] American Society of Mechanical Engineers, ASME Pressure Vessel and Boiler Code, New York (1989).

[11.64] K Wallin, Descriptive potential of Charpy V fracture arrest parameter with respect to crack arrest K_{Ia}, VTT, Metals Laboratory, VTT-MET B-221 (1993).

[11.65] T Planman, K Wallin and R Rintamaa, Comparison of some indirect measures of crack arrest, Conference on crack arrest concepts for failure prevention and life extension, Abington, Cambridge (1995).

[11.66] T S Robertson, Propagation of brittle fracture in steel, J Iron and Steel Institute **175**, 361-374 (1953).

[11.67] R W Nichols, Fast and brittle fracture studies related to steel pressure vessels, Proc Roy Soc Lond **285A**, 104-119 (1965).

[11.68] C S Wiesner, Predicting structural crack arrest behaviour using small-scale material characterisation tests, Int J Pres Ves Piping **69**, 185-196 (1996).

[11.69] M R Baum, Axial rupture of large diameter, gas pressurised, steel pipes, Int J Pres Ves Piping **21**, 21-48 (1985).

11.4 Consideration of proof testing and warm prestressing

11.4.1 Introduction

This section describes how the loading history due to i) proof or overload tests or ii) warm pre-stressing of a structure containing flaws may be taken into account when performing an integrity assessment using the Fracture Procedures described in this document. The effect of loading history is considered with regard to mechanical relaxation of residual stresses and enhancement of lower shelf fracture resistance. The latter is only applicable where the pre-load constitutes a warm pre-stress.

Procedures are set out below which enable these effects to be quantified. In practice, the different phenomena may interact and it may not be possible to separate the different effects simply.

11.4.2 Proof or overload testing

In the assessment of a cracked component that has been proof tested, the residual stress level assumed in the fracture analyses can be taken [11.70] as the lower of:

$$\sigma'_{\mathrm{Y}}, \text{ or } \left(1.4 - \frac{\sigma_{\mathrm{ref}}}{\sigma'_{\mathrm{f}}}\right)\sigma'_{\mathrm{Y}} \qquad (11.10)$$

where

σ_{ref} is the reference stress under the proof load conditions;

σ'_{Y} is the appropriate material yield strength at the proof test temperature; and

σ'_{f} is the flow strength (assumed to be the average of the yield and tensile strengths) at the proof test temperature. Note that the assumed residual stress level should always be ≥ 0.

Where a crack in a proof loaded structure is believed to have initiated in service, after the proof loading, the residual stress level in fracture analysis should be taken as [11.71] the lower of

$$\sigma_{\mathrm{Y}}, \text{ or } \left(1.1\,\sigma'_{\mathrm{Y}} - 0.8\sigma_{\mathrm{a}}\right) \qquad (11.11)$$

where σ'_{Y} is the appropriate material yield strength at the proof test temperature and σ_{a} is the applied stress due to the proof loads at the location of interest. σ_{a} is a stress normal to the plane of the flaw and should be taken as the lower of the membrane stress in the section containing the location of interest, or the total stress at the location of interest including membrane, bending and stress concentration effects. The total stress can be lower than the membrane stress if the bending stress is negative or if there is a stress de-concentration effect, such as at the convex side of a welded joint with angular misalignment.

11.4.3 Warm prestressing

A warm pre-stress (WPS) is an initial pre-load applied to a ferritic steel structure containing a pre-existing flaw which is carried out at a temperature above the ductile-brittle transition temperature, and at a higher temperature or in a less-embrittled state than that corresponding to the subsequent service assessment. A WPS argument differs from a proof-test argument in conferring added resistance to fracture under the assessment conditions; that is, it is considered to elevate the stress intensity factor at failure, K_f, above the corresponding fracture toughness, K_{mat}, in the absence of the WPS [11.72-11.83].

In service assessments using the procedure given in Section 6, the fracture toughness used in evaluating K_r is then taken as the enhanced value K_f.

There are basically three types of cycle which are used in the laboratory to demonstrate the WPS effect (Fig. 11.10). The temperatures at which the pre-load and re-load to failure occur are denoted by T_1 and T_2, respectively, in each case. Similarly, the stress intensity factors due to the pre-load and following removal of the load are denoted K_1 and K_2, respectively.

a) Load-Unload-Cool-Fracture (LUCF), where the structure is pre-loaded at temperature T_1 to stress intensity factor K_1, unloaded to stress intensity factor K_2, cooled to temperature T_2 and re-loaded to fracture. The case where $T_2 = T_1$ is permissible if hardening mechanisms have occurred prior to the re-load to fracture.

b) Load-Cool-Unload-Fracture (LCUF), where cooling to T_2 takes place prior to unloading and re-loading to fracture.

c) Load-Cool-Fracture (LCF). This is similar to the LUCF cycle except that no unloading occurs prior to the imposition of extra load to fracture.

The greatest benefit in terms of maximising K_f is given by the LCF cycle, the least by the LUCF cycle with full unloading. Intermediate forms of cycle, where partial unloading occurs prior to re-loading to failure, and where the temperature and pressure are simultaneously reduced, give benefits lying between these two limits.

This sub-section gives advice on quantifying the benefit of a WPS. Two levels of argument are set out: firstly, a simplified lower-bound approach; and secondly, a more detailed route based on calculations, which may be of value when the simplified route is insufficient.

For a WPS argument to be made according to the procedure of this section, the following conditions should be met:

a) The failure mechanism at the service condition must be transgranular cleavage or intergranular brittle fracture [11.73].

b) The flow properties of the material should increase between the WPS and the service failure condition; this may be due to a decrease in temperature or due to in-service hardening.

c) There should be no significant sub-critical crack growth between the WPS and the service failure condition. The amount of any such crack growth should be much less than the extent of the residual plastic zone following unloading [11.83, 11.84]. Approximate formulae for estimating this plastic zone size is given in [11.74-11.76].

d) The stress intensity factor K_1 due to the WPS loading should exceed the fracture toughness K_{mat} at the re-load condition.

e) Small-scale yielding conditions hold, that $\left(K_I / \sigma_{Y1}\right)^2 / 2\beta\pi$ is much less than the size of the un-cracked ligament and any relevant structural dimensions. Here σ_{Y1} is the yield strength at the pre-load and β=1 or 3 in plane stress or plane strain, respectively.

There is evidence [11.72, 11.76, 11.84] that, for increasing pre-loads, the benefits on the apparent re-load fracture toughness lessen. Indeed, in the limit of extensive plasticity, the toughness may actually be reduced compared to its value in the absence of the WPS. References [11.72, 11.76] should be consulted for further advice in cases of large pre-loads.

f) The pre-load and re-load should be in the same direction; that is, both tensile or both compressive at the crack tip. A compressive pre-load followed by a tensile re-load may reduce the apparent fracture toughness.

11.4.3.1 Simplified WPS argument

Failure is avoided if the stress intensity factor during cooling is constant or monotonically falling to a value K_2. This is often referred to as the 'conservative warm pre-stressing principle'. A benefit is obtained if K_2 exceeds the fracture toughness in the absence of a WPS, K_{mat}, and is consistent with maximum benefit from an LCF cycle. Margins against failure are not given by this simplified argument. In order to quantify margins it is necessary to use the detailed approach of Section 11.4.3.2.

A particular example of this simplified WPS argument is in the assessment of thermal downshocks (such as a pressurised thermal shock or PTS transient in a steel reactor pressure vessel), where brittle fracture would otherwise be conceded [11.73, 11.82]. The loading history during the thermal shock event is regarded as a WPS. It is argued that failure does not occur when the instantaneous stress intensity factor K_I exceeds the corresponding K_{mat} if K_I is then reducing with temperature. The maximum size of flaw which satisfies this criterion can then be compared with the size of the largest flaw which may have escaped detection to derive a margin on crack size. Any sub-critical growth of the latter flaw between inspection and the service assessment time should be allowed for.

Some experimental validation of the simplified WPS argument applied to pressurised thermal shock events is presented in [11.73, 11.82].

11.4.3.2 Full WPS procedure

The procedure is based on the model of [11.80]. It includes an interpolation between the bounding cases of LUCF with full unloading and the LCF cycle. The fracture toughness used in service assessments using the procedure of the main text is then K_f.

The following steps should be carried out in quantifying the effect of the WPS on K_f for a given structural geometry and flaw dimensions:

(1) Determine the temperature and load level corresponding to the WPS.

(2) Determine the stress intensity factor decrement due to the unload, $\Delta K_u = K_1 - K_2$. It follows that ΔK_u is independent of the magnitude of any system or residual stresses incorporated in the total stress intensity factors K_1 and K_2 at the pre-load and unload phases, and depends on the contribution due to the varying load only.

(1) Evaluate the fracture toughness, K_{mat}, of the material at the assessment time, but neglecting the effects of the WPS. The effects of any degrading mechanism, such as strain ageing or irradiation embrittlement which may have occurred between the time of the WPS and the subsequent assessment should be taken into account. A lower bound value of K_{mat} should be adopted both for consistency with the procedures of the main document and to conservatively predict the elevation in K_f (see equation (11.12) below).

(3) Evaluate the stress intensity factor at failure from:

$$K_f = K_2 + \sqrt{K_{mat}\Delta K_u} + 0.15K_{mat} \qquad (11.12)$$

when $K_{mat} < \Delta K_u$. If $K_{mat} \geq \Delta K_u$ then the conditions $K_2 = K_1$ and $\Delta K_u = 0$ are imposed in equation (III.10.1). If the calculated $K_f \leq K_{mat}$ then no WPS benefit is estimated and $K_f = K_{mat}$.

No additional benefit should be claimed from repeated applications of a WPS as experimental data suggest no significant further effect [11.78, 11.84]. Similarly, benefit should not be claimed from both residual stress reduction due to a WPS and an apparent enhancement in K_f using this section [11.78, 11.84].

11.4.3.3 The WPS effect

The benefits of a WPS in thick-section components have been attributed [11.73] mainly to the establishment of a compressive residual stress zone ahead of the crack tip. However, the effects of crack-tip blunting and strain hardening have also been claimed as significant by a number of authors. Experimental demonstration of the WPS effect has been reported in many references [11.73, 11.80, 11.82] using both small specimen and feature tests. A number of alternative quantitative models of WPS benefits have been developed. These include both 'global' models based on crack driving force [11.72, 11.74-11.76] and energetic [11.85] considerations, and 'local' models [11.73, 11.86, 11.87] which use local approach methods (Section III.9). Validation of the model predictions against both specimen and large-scale test data is summarised in, for example, [11.73, 11.82].

The previous issue of this section restricted the application of WPS to transgranular cleavage fracture, consistent with the conclusions of [11.74]. However, it has been argued [11.73] that this restriction is unnecessary and that a WPS benefit both exists in the case of failure by stress-controlled intergranular brittle fracture mechanisms and may also be quantified using existing WPS models. There is experimental evidence for this assertion [11.81, 11.88]. Hence the restriction on fracture mode has been relaxed at this issue.

Some applications of the simplified WPS argument of Section 11.4.3.1 [11.89] have used the crack driving force $K_J = \sqrt{E'J}$ based on J estimated using Section 5.4.4, rather than K_I. K_J was compared with the fracture toughness curve during the entire pressurised thermal shock (PTS) event, enabling tearing under rising load to be excluded prior to WPS benefit on unloading. This usage is consistent with Section 11.4.3.1 as, for practical PTS load histories, K_J decreases when K_I decreases on cooling.

Equation (11.12) was shown [11.80] to predict similar results to the detailed models in [11.74-11.76]. These detailed models include a dependence on yield stress. Approximate estimates of K_f may also be calculated using a simpler model [11.74] which does not contain an explicit dependence on yield stress. Similar simple and more complex expressions are also given in [11.72, 11.77]. The simple models were recommended in the previous issue of this section and were based on consideration of the bounding LUCF cycle. Equation (11.12) allows for the range of cycles between LUCF and LCF to be considered. It was shown [11.80] to give a lower bound to a large body of test data when used with lower bound estimates of K_{mat}, and a good fit to the overall test data when using median toughness data.

The restriction to limit sub-critical crack growth between the WPS and loading to failure is based on modelling [11.83] and experimental observation [11.73, 11.79]; under this condition no deleterious effect was found. When significant fatigue crack growth occurred by cycling to a lower load following unload to K_2, [11.80] showed that good agreement between equation (11.12) and the experimental failure loads could be achieved for two particular test data by substituting K_2 for K_1. Use of the unmodified K_1 was non-conservative.

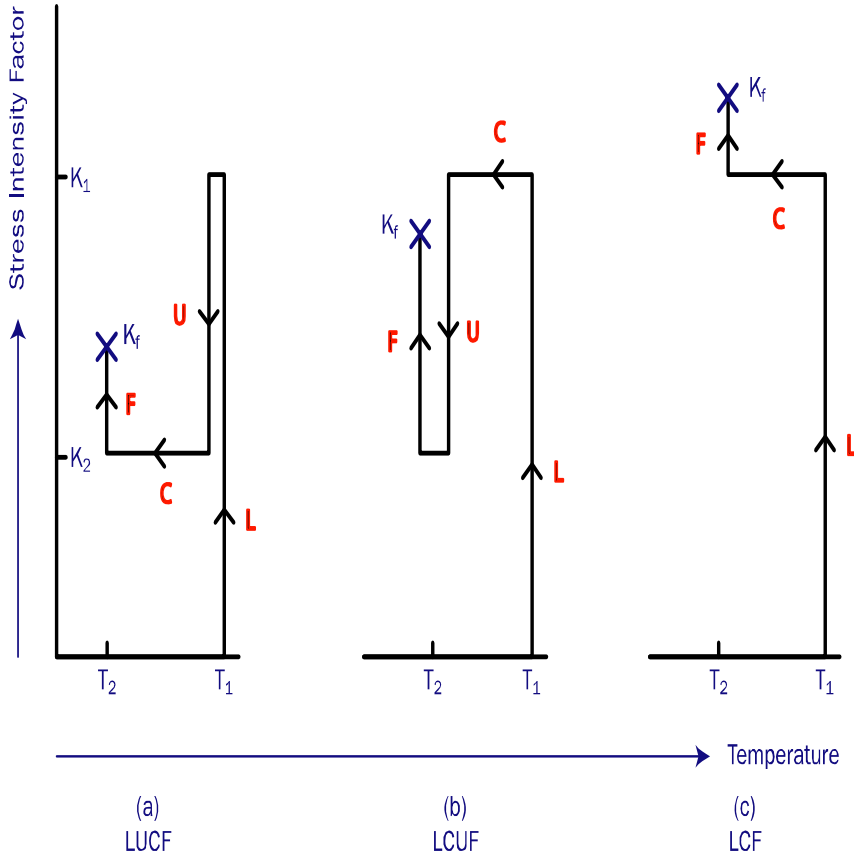

Figure 11.10 –Typical laboratory warm pre-stress cycles

(a) LUCF (b) LCUF (c) LCF

11.4.4 Bibliography

[11.70] R.H. Leggatt, 1988. Investigations of proposed procedures for the inclusion of residual stresses in the revised fracture sections of PD 6493. In: Proc of International Conference on Residual Stresses (ICRS2), Nancy, France, 23-25 November 1988.

[11.71] LEGGATT, R.H. and T.G. DAVEY., 1988. Measurements of the reduction due to proof loads of residual stresses in simulated pressure vessel welds. *In:* L. MORDFIN, ed. *Mechanical relaxation of residual stresses. Proc. International symposium on mechanical relaxation,* Cincinnati, Ohio, 30 April 1987. Philad D

[11.72] J Smith and S J Garwood, The significance of prior overload on fracture resistance: a critical review, Int J Pres Ves Piping 41, 255-296 (1990).elphia: ASTM. STP 993, 30-41. ISBN 0803111665

[11.73] D J Smith, The influence of prior loading on structural integrity, Chapter 8, Volume 7, 289-345, Comprehensive Structural Integrity, Elsevier (2003).

[11.74] G G Chell and J R Haigh, The effect of warm prestressing on proof tested pressure vessels, Int J Pres Ves Piping 23, 121-132 (1986).

[11.75] G G Chell, Some fracture mechanics applications of warm pre-stressing to pressure vessels, Proc 4th Int Conf on Pressure Vessel Technology, Vol.1, 117-124 (1980).

[11.76] G G Chell and D A Curry, Mechanics and mechanisms of cleavage fracture, Section 8 'Generalised loading', in 'Developments in fracture mechanics-2', G G Chell (editor), Appl Sci (London), 161-177 (1981).

[11.77] D J Smith and S J Garwood, Application of theoretical methods to predict overload effects on fracture toughness of A533B, Int J Pres Ves Piping 41, 333-357 (1990).

[11.78] F M Burdekin and D P G Lidbury, Views of TAGSI on the current position with regard to benefits of warm prestressing, Int J Pres Ves Piping 76, 885-890 (1999).

[11.79] H J Fowler, The influence of warm pre-stressing and proof loading on the cleavage fracture toughness of ferritic steels, PhD Thesis, University of Bristol (1998).

[11.80] K Wallin, Master Curve implementation of the warm pre-stress effect, Engng Fract Mech 70, 2587-2602 (2003).

[11.81] J Cheng and F W Noble, The warm prestressing effect in steels undergoing intergranular fracture, Fatigue Fract Engng Mater Struct 20, 1399-1411 (1997).

[11.82] D P G Lidbury, A H Sherry, C E Pugh and B R Bass, The performance of large-scale structures and validation of assessment procedures, Chapter 14, Volume 7, 529-566, Comprehensive Structural Integrity, Elsevier (2003).

[11.83] G G Chell, The effects of sub-critical crack growth on the fracture behaviour of cracked ferritic steels after warm prestressing, Fatigue Fract Engng Mater Struct 9, 259-274 (1986).

[11.84] Muhammed, A. 1998. 'The effect of prior overload and its application in structural integrity assessments' TWI Report SINTAP/TWI/014, March 1998.

[11.82] Y Wadier and M Bonnamy, The energy approach of elastic-plastic fracture mechanics applied to the analysis of the warm pre-stress effect, ASME PVP 461, 89-96 (2003).

[11.86] A Pineau, Practical application of local approach methods, Chapter 5, Volume 7, 177-225, Comprehensive Structural Integrity, Elsevier (2003).

[11.87] W Lefevre, G Barbier, R Masson and G Rousselier, A modified Beremin model to simulate the warm pre-stress effect, Nucl Engng Design 216, 27-42 (2002).

[11.88] G Gage, J P Jackson, P H Ray and D R Wigham, Warm prestressing in pressure vessel steels: comparison of the effect of cleavage and intergranular fracture modes and the use of small specimens, AEA Technology Report AEAT-0919 (1996), including supplementary appendix by G Gage (1998).

[11.89] C J Gardner, Sizewell 'B' power station – revised integrity assessment for the end-of-life safety case for the reactor pressure vessel IoF pressure boundary, BEGL Report E/REP/STAN/0057/SXB/01 (2001).

11.5 Evaluation under Mode I, II and III Loads

Lead drafter:	Peter Budden – British Energy & Anssi Laukkanen - VTT
Lead commentators:	
Word file	**Mixed-mode** 22 March 06.doc

11.5.1 Introduction

This section gives guidance on flaw evaluation under Mode I, II and III loads. These loading modes are as defined in Figure 11.11. The guidance is reproduced from R6.

This section is used when shear stresses in the plane of the flaw must be considered. Advice on reference planes for flaw characterisation is given in Annex E and, except in the case when principal planes are used, shear stresses need to be taken into account. The definition of an effective stress intensity factor, K_{eff}, for use in defining K_r is set out and distinguishes between materials where $K_{mat}/\sigma_y < 0.2$ m^{½} and those where $K_{mat}/\sigma_y \geq 0.2$ m^{½}. This should be considered particularly for sensitivity analyses where material properties are varied.

Compared to pure Mode I loading, shear loadings and mixed mode loadings tend to produce lower hydrostatic stresses but higher strains near the crack tip [11.90-11.93]. A mechanistic understanding of mixed mode loading requires these stress and strain fields to be combined with a detailed knowledge of the failure micromechanism [11.91]. This section therefore recommends an assessment route based upon Mode I material property values K_{mat} and σ_y and Mode I failure assessment diagrams. The Mode II and III contributions are incorporated in the calculation of the applied stress intensity factors, K_{eff}, and the plastic limit load. The justification for this is empirical and discussed in Section 11.5.5. The reader is cautioned to read these and assess the validity of the analysis accordingly.

The procedures are, in principle, those outlined in Section 6. However, it is advised that the approach is limited to an initiation analysis only, because of uncertainty and complications about the plane of the growing crack (Section 11.5.5). The individual steps in the procedure of Section 6 are not repeated here but advice on specific issues is contained in the following sections.

11.5.2 Failure Assessment Diagrams for use in Modes I, II and III

Mode I diagrams are generally found to be representative of those derived for Mode II and Mode III [11.94, 11.95], although theoretical evidence exists that under some circumstances these diagrams may not be conservative [11.95]. Any differences are similar to those observed between various Mode I curves and therefore the curves of Section 6 are also recommended for use in assessments under Mode II and III loads. The Option 1 diagram in particular is recommended for use in mixed mode loading assessments.

Under mixed mode loading there is less validation for the failure assessment curves [11.92, 11.96, 11.97] and therefore use of these curves should be in conjunction with a sensitivity analysis.

11.5.3 Evaluation of K_r

In Section 5, the applied stresses are resolved into σ^p (primary) and σ^s (secondary) type stresses. Under Mode I loading the value of K_r is the sum of two components, K_r^p and K_r^s, corresponding to the σ^p and σ^s stress categories. Under combined Mode I, II and III loading this simple addition is no longer valid and the linear dependence of K_r on applied load is lost.

In view of the problems in the analysis of ductile crack growth under mixed mode loading (see Section 11.5.4) advice is given only for the evaluation of K_r for an initiation analysis. In addition, consideration of fatigue crack growth, creep crack growth and environmentally assisted cracking is outside the scope of this section.

11.5.3.1 Linear Elastic Stress Intensity Factor

Stress intensity factors may be determined using general calculation methods. In the absence of accurate compliance functions for mixed mode loading, Mode I values can be used to provide pessimistic estimates. When dealing with flaws subject to mixed mode loading, the situation can either be analysed directly or the flaw can be projected onto a reference plane. In the latter case however, unless the principal planes are chosen, shear stresses must be taken into account in the evaluation of stress intensity factors.

In general the stress intensity factors (SIF) for tensile (Mode I), in-plane shear (Mode II) and out-of-plane shear (Mode III) loadings are required in the calculation of K_r.

These are designated as follows:

K_I^p (a) and K_I^s (a) - the linear elastic SIFs for the flaw size, a, for loads giving rise, respectively, to σ^p and σ^s stress components which are normal to the plane of the crack.

$\mathrm{K}_{\mathrm{II}}^{\mathrm{p}}$ (a) and $\mathrm{K}_{\mathrm{II}}^{\mathrm{s}}$ (a) - the linear elastic SIFs for the flaw size, a, for loads giving rise, respectively, to σ^p and σ^s stress components which are in-plane shear.

$\mathrm{K}_{\mathrm{III}}^{\mathrm{p}}$ (a) and $\mathrm{K}_{\mathrm{III}}^{\mathrm{s}}$ (a) - the linear elastic SIFs for the flaw size, a, for loads giving rise, respectively, to σ^p and σ^s stress components which are out-of-plane shear (torsion).

In addition, it is necessary to evaluate the parameter $\rho(a)$, which takes account of plasticity corrections required to cover interactions between σ^p and σ^s stresses (see Section 6). A method of evaluating ρ is given in Section 11.5.3.4.

11.5.3.2 The Effective Stress Intensity Factor

As advice is given only for initiation analyses for mixed mode fracture assessments, the crack size, a, is the size of the original flaw, a_o.

Determine the three SIF components K_I, K_{II}, and K_{III} as follows:

$$\begin{aligned}\mathrm{K_I} &= \mathrm{K_I^p} + \mathrm{K_I^s}\\ \mathrm{K_{II}} &= \mathrm{K_{II}^p} + \mathrm{K_{II}^s}\\ \mathrm{K_{III}} &= \mathrm{K_{III}^p} + \mathrm{K_{III}^s}\end{aligned} \qquad (11.13)$$

Hence calculate the effective SIF, K_{eff}, as follows:

(a) If $\mathrm{K_{mat}}/\sigma_y \geq 0.2\sqrt{\mathrm{m}}$

$$\mathrm{K_{eff}} = [\mathrm{K_I^2} + \mathrm{K_{II}^2} + \alpha \mathrm{K_{III}^2}/(1-\nu)]^{1/2} \qquad (11.14)$$

where α = 1, in general.

(b) If $K_{mat}/\sigma_y < 0.2\sqrt{\mathrm{m}}$

and there are specific material data to justify that $K_{IIC} > K_{mat}$, then equation (11.14) should be used to define K_{eff}. If $K_{IIC} < K_{mat}$, or if there is insufficient evidence to assert otherwise, then K_{eff} should be evaluated as follows:

$$K_{eff} = [(K_{12})^2 + \alpha\ K_{III}^2\ /(1-\nu)]^{1/2} \quad (11.15)$$

where

$$K_{12} = \frac{\left\{2K_I + 6\sqrt{K_I^2 + 8K_{II}^2}\right\}}{8}\left\{\frac{K_I^2 + 12K_{II}^2 + K_I\sqrt{K_I^2 + 8K_{II}^2}}{2K_I^2 + 18K_{II}^2}\right\}^{3/2} \quad (11.16)$$

$$\text{for } |K_I / K_{II}| \geq 0.466, \text{and}$$

$$K_{12} = \frac{|K_{II}|}{0.7} \quad (11.17)$$

$$\text{for } |K_I / K_{II}| < 0.466$$

with α = 1 in general.

For metallurgically brittle fracture it is sometimes possible to neglect the contribution of the Mode III stresses. In cases where this can be justified from available experimental data the parameter α can be set equal to zero and the justification should be reported.

11.5.3.3 Evaluation of K_r for an Initiation Analysis

$$K_r = K_{eff}(a_o) / K_{mat} + \rho(a_o) \quad (11.18)$$

where ρ is defined in Section 11.5.3.4 below.

11.5.3.4 Procedure for the Evaluation of ρ

In the absence of firm knowledge concerning the interaction of σ^P and σ^S stresses in different modes the procedure of Section 6 is adopted with an effective SIF replacing the Mode I SIF as follows:

a) For the elastically calculated σ^s stresses for the crack size of interest, define K_{eff}^s from equations (11.14) or (11.15), as appropriate, depending on the values of K_{mat}/σ_y, K_I/K_{II} and K_{IIC}/K_{mat}, with K_I, K_{II}, K_{III} in equations (11.14) - (11.17) replaced by $K_I^s, K_{II}^s,$ and K_{III}^s, respectively.

(b) For the σ^p stresses define K_{eff}^p from equations (11.14) or (11.15) as appropriate, depending on the values of K_{mat}/σ_y, K_I/K_{II} and K_{IIC}/K_{mat}, with K_I, K_{II}, K_{III} in equations (11.14) - (11.17) replaced by K_I^p, K_{II}^p and K_{III}^p, respectively.

Evaluate the ratio (K_{eff}^p / L_r). For multiple loading systems in which the various σ^p loads increase independently (non-proportionally), both K_{eff}^p and L_r depend on the ratios of the independent loads. Thus the value of (K_{eff}^p / L_r) must be calculated for each load combination of interest when, for example, assessing individual load factors.

(c) Evaluate $K^{s}_{eff} / (K^{p}_{eff} / L_r)$ from the results of (a) and (b).

(d) Evaluate ρ according to the procedures of Section 6 replacing K_I by K_{eff}.

11.5.4 Evaluation of Lr

The parameter L_r is a measure of how close the structure containing the flaw is to plastic collapse. The applied loads to be used in evaluating L_r are those which give rise to σ^p stresses. L_r is defined as the ratio of the loading condition being assessed to the limit load of the structure:

$$L_r = \frac{\text{total applied load giving rise to } \sigma^p \text{ stresses}}{\text{limit load of the flawed structure}} \qquad (11.19)$$

For multiple loading systems, $(1/L_r)$ is the factor by which the loads of interest giving rise to σ^p stresses must be increased in order for the limit load of the flawed structure to be attained.

The value of σ_y used in evaluating L_r is that obtained from uniaxial tensile data. The von Mises yield criterion is recommended for shear or multiaxial stress fields.

The limit load review of Miller [11.98] contains a number of solutions which involve multiaxial and shear loadings. In addition Ewing [11.99, 11.100] has presented a number of solutions for extended flaws under mixed Mode I/Mode II loadings. In other cases values of L_r can be obtained by following general methods of limit analysis.

11.5.5 Further Information

A particular problem that arises in mixed mode assessments is that there are no universally accepted methods of fracture toughness testing other than those for Mode I loading. Testing methods for pure Mode II loading [11.101, 1.102] and pure Mode III loading [11.103, 11.104] were proposed in the early 1980's. However, interpretation of the resulting load-deflection curves is difficult, and the results can generally be used only to indicate whether or not the toughness is greater than that under Mode I loading. More recent workers have performed extensive cracked body finite element analyses for particular mixed mode specimen designs in order to develop mixed mode J-integral solutions [11.105-11.110]. However, no consensus has emerged on the best specimen design or test procedure, and it is evident that the load and displacement boundary conditions applied to a mixed mode test specimen are more difficult to define or control than the much simpler Mode I conditions [11.109,11.111].

Theoretical analysis can give some indication of expected behaviour. For pure Mode III loading it is difficult to achieve brittle fracture so that the fracture toughness under these conditions would be expected to be greater than that under Mode I [11.91, 11.112]. Under such circumstances it may be possible to neglect the Mode III contribution to fracture. However, a conservative approach is adopted in this section which generally includes the contribution from Mode III, unless the user can demonstrate by available experimental evidence that such a contribution can be neglected.

Similarly, for brittle fracture under Mode II or mixed Mode I/Mode II the toughness would be expected to be greater than under Mode I, except for some special circumstances where crack tip plasticity is very small [11.91, 11.113]. The available experimental evidence supports this and suggests that for Mode II or mixed Mode I/Mode II the special circumstances only arise at very low temperatures (-200ºC) for common structural steels, or at ambient temperatures in very high strength/low toughness steels [11.91, 11.96, 11.114, 11.115]. Thus, this section has pessimistically adopted the use of the Mode I toughness for assessment purposes in the brittle fracture region, except for the special cases where $K_{mat} / \sigma_y < 0.2\sqrt{m}$.

Finite element studies of mixed Mode I/II loading [11.92, 11.93] indicate that the introduction of shear loading causes effects similar to in-plane constraint loss in Mode I, namely a reduction in the peak direct and hydrostatic stresses in the vicinity of the crack tip. This promotes a transition from cleavage fracture near Mode I to ductile fracture near Mode II [11.114, 11.115]. There may thus be considerable pessimism in mixed-mode assessments performed according to this procedure on steels in the lower transition region.

The evidence from mixed Mode I/II fracture testing of ductile materials is confusing, with some workers reporting a Mode II initiation toughness and crack growth resistance the same or higher than the Mode I equivalent [11.102, 11.105, 11.108, 11.116-11.121], and others reporting a lower Mode II initiation toughness and crack growth resistance [11.106, 11.107, 11.110, 11.122-11.125]. Some of this variability in behaviour may be due to the difficulties inherent in mixed mode fracture testing. Despite this reservation, there is close qualitative agreement between the results of recent studies on structural steels tested using three different specimen designs [11.106, 11.107, 11.110, 11.124]. All show a steady fall in the ductile crack growth resistance curve as the proportion of Mode II loading increases, with the lowest resistance curve obtained for pure or nearly pure Mode II loading. This fall in apparent fracture resistance is associated with a change in the mechanism of fracture. Near Mode I the crack blunts symmetrically and crack growth takes place by the classical void coalescence and growth mechanism; while near Mode II the crack blunts asymmetrically and crack growth takes place by a shear band mechanism from the sharpened side of the crack tip. These experimental observations are supported by theoretical modeling using finite element methods [11.93].

The procedure adopted in this section is based on the use of the Mode I fracture toughness with a simple sum of the squares of the stress intensity factors [11.91, 11.96, 11.97]. At first sight this recommendation is not consistent with the experimental results and theoretical modeling cited above. However, the testing performed by Swankie [11.110] has been assessed using the methods of this section [11.111], with the finding that the lower mixed mode and Mode II ductile crack growth resistance curves are always associated with specimens tested at loading levels beyond the collapse cut-off, $L_r^{\max}$.

The approach given here is limited to initiation analyses. The analytical and experimental studies of stable crack growth under combined tensile and shear loading are limited and complicated by crack growth often occurring at an angle to the direction of the original crack. Any analysis involving ductile crack growth under these circumstances, therefore, requires justification of the resistance curve data adopted. It is not possible at present to recommend general methods, although successful mixed mode tearing analyses have been performed [11.111].

Using the results of J-analysis, the failure assessment curves relevant to pure Mode II and pure Mode III loading have been obtained and compared with the Mode I curves of Option 1 and Option 2 [11.94, 11.95]. On this basis the failure assessment curves originally developed for Mode I loading are also recommended for other loading modes. However, the analytical evidence, particularly for small cracks, suggests that under some circumstances the Mode III curves lie inside the Mode I diagram. It is judged that sufficient conservatism exists in the procedures to account for these variations, but it should be recognised that the validation under mixed mode loading is very limited and, therefore, a thorough sensitivity analysis is required.

11.5.6 Bibliography

[11.90] C F Shih, Small-scale yielding analysis of mixed mode plane-strain crack problems, in Fracture Analysis, ASTM STP 560, 187-210 (1974).

[11.91] P J Budden and M R Jones, Mixed mode fracture, CEGB Report RD/B/6159/R89 (1989).

[11.92] Z Z Du, C Betegon and J W Hancock, J dominance in mixed mode loading, Int J Fract **52**, 191-206 (1991).

[11.93] A H Sherry, M A Wilkes and R A Ainsworth, Numerical modelling of mixed-mode ductile fracture, ASME PVP-Vol 412, ASME Pressure Vessels and Piping Conference, Seattle, 15-24 (2000).

[11.94] R A W Bradford, A summary of mode II failure assessment diagrams for Carbon-Manganese steels, CEGB Report SWR/SSD/0631/N/85 (1985).

[11.95] R A W Bradford, A discussion of failure assessment diagrams in mode III, CEGB Memorandum SWR/SSD/S/1536/S/85 (1985).

[11.36] G Green, Monotonic fracture under mixed mode loading: a review of experimental data and the implications for structural integrity assessment, CEGB Report SWR/SSD/0632/R/85 (1985).

[11.97] D W Dean, Analysis of mixed mode fracture data using the CEGB failure assessment procedure, CEGB Report SER/SSD/86/0018/N (1986).

[11.98] A G Miller, Review of limit loads of structures containing flaws – 3rd Edition, CEGB Report TRPD/B/0093/N82 - Rev 2 (1987).

[11.99] D J F Ewing, Plastic yielding under combined tensile/shear loading, CEGB Report TPRD/L/2360/N82 (1982).

[11.100] D J F Ewing and J N Swingler, Plastic yielding of an edge cracked section in the presence of shear, CEGB Report TPRD/L/2770/N84 (1985).

[11.101] L Miles, Development of a mode II fracture toughness testing procedure for an elastic-plastic material, CEGB Report SSD/SW/R395 (1982).

[11.102] M Chant, G Green, I J Whatmough and D C Williams, The first large shear specimen test, CEGB Report SWR/SSD/0250/R/83 (1983).

[11.103] N Tsangranis, Fracture behaviour of 4340 steel under mode III loading, Engng Fract Mech **16**, 569 (1979**).**

[11.104] M Yoda, The J-integral fracture criterion under opening and tearing modes and unloading effects, Engng Fract Mech **13**, 647-656 (1979).

[11.105] K Tohgo and H Ishii, Elastic-plastic fracture toughness test under mixed mode I-II loading, Engng Fract Mech **41**, 529-540 (1992).

[11.106] A Laukkanen, K Wallin and R Rintamaa, Evaluation of the effects of mixed mode I-II loading on elastic-plastic ductile fracture of metallic materials, Mixed-Mode Crack Behaviour, ASTM STP 1359 (1999).

[11.107] A Pirondi and C Dalle Donne, Mixed mode fracture of a ferritic steel: J-integral against CTOD, 5th Int Conf on biaxial/multiaxial fatigue and fracture, Cracow, Poland (1997).

[11.108] S Aoki, K Kishimoto, T Yoshida, M Sakata, and H A Richard, Elastic-plastic fracture of an aluminium alloy under mixed mode loading, J Mech Phys Solids **38**, 2, 195-213 (1990).

[11.109] M R Ayatollahi, Geometry and constraint effects in mixed mode fracture, PhD Thesis, University of Bristol (1998).

[11.110] T D Swankie, The role of shear and constraint in mixed mode fracture, PhD Thesis, University of Bristol (1999).

[11.111] M C Smith, The application of R6 appendix 7 to mixed mode fracture tests of a pressure vessel steel, British Energy Generation Report E/REP/GEN/0022/00 (2000).

[11.112] J Phillips, The prediction of fracture toughness for a pressure vessel steel under mode 3 loading, CEGB Report RD/B/5224N81 (1981).

[11.113] R A Ainsworth and R P Harrison, Application of the CEGB failure assessment route in the presence of shear loading, CEGB Report RD/B/5022N81 (1981).

[11.114] T D Swankie and D J Smith, Low temperature mixed mode fracture of a pressure vessel steel subject to prior loading, Engng Fract Mech **61**, 387-405 (1998).

[11.115] D J Smith, M R Ayatollahi, J C W Davenport and T D Swankie, Mixed mode brittle and ductile fracture of a high strength rotor steel at room temperature, Int J Fract **94**, 235-250 (1998).

[11.116] B Cotterell, E Lee and Y M Mai, Mixed mode plane stress ductile fracture, Int J Fract **20**, 243-250 (1982).

[11.117] M Chant, G Green and D C Williams, The second large shear specimen test, CEGB Report SWR/SSD/0344/N/83 (1983).

[11.118] Y W Shi, N N Zhou, and J X Zhang, Comparison of mode I and mode II elastic-plastic fracture toughness for two low alloyed high strength steels, Int J Fract **68**, 89-97 (1994).

[11.119] L Banks-Sills and D Sherman, J_{II} fracture testing of a plastically deforming material, Int J Fract **50**, 15-26 (1991).

[11.120] M Yoda, The effect of notch root radius on the J-integral fracture toughness under mode I, II, and III loadings, Engng Fract Mech **26**, 3, 425-431 (1987).

[11.121] Sha Jiangbo, Sun Jun, Zhu Pin, Deng Zengjie and Zhou Huijiu, Study on the behavior of elastic-plastic fracture under mixed mode loading in aluminum Ly12 – J-integral analysis, Int J Fract **102**, 141-154 (2000).

[11.122] T M Maccagno and J F Knott, The mixed mode I/II fracture of lightly tempered HY130 steel at room temperature, Engng Fract Mech **41**, 6, 805-820 (1992).

[11.123] D Bhattacharjee and J F Knott, Ductile fracture in HY100 steel under mixed mode I/mode II loading, Acta Met **42**, 5, 1747-1754 (1994).

[11.124] J C W Davenport and D J Smith, Mixed mode ductile tearing in a ferritic steel, Proc. ECF10, Vol. 2, EMAS, 901-910 (1994).

[11.125] K Tohgo, K Otsuka, and H-W Gao, Behaviour of ductile crack initiation from a crack under mixed mode loading, J Soc of Mater Sci Japan **39**, 443, 1089-1094 (1990).

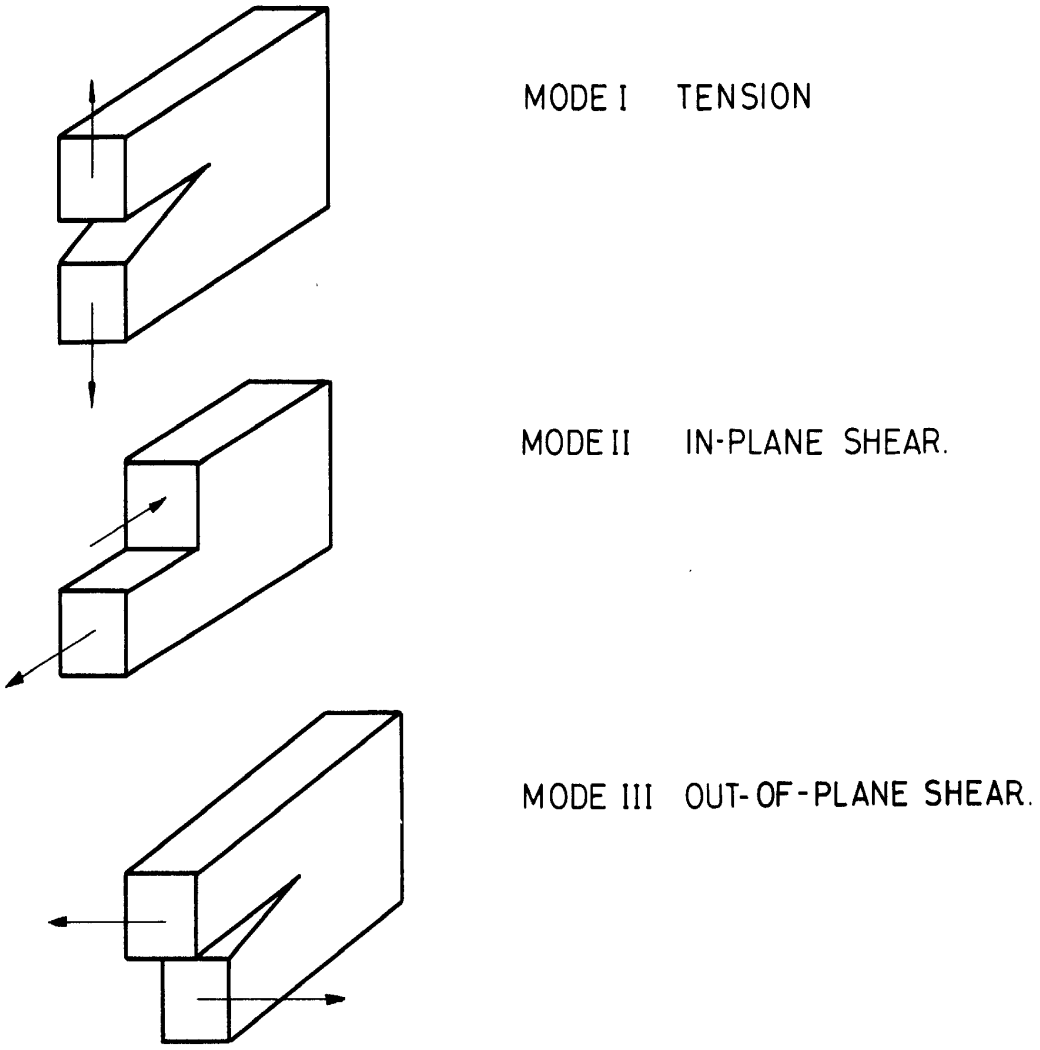

Figure 11.11 – Definitions of loading modes

11.6 Master curve

Lead drafter:	Kim Wallin – VTT
Lead commentators:	
Word file	**Master curve** 15 Feb 05.doc

11.6.1 Introduction

The Master Curve method is a statistical, theoretical and micromechanism based analysis method for fracture toughness in the ductile to brittle transition region. The method, originally developed at VTT Manufacturing Technology [11.126], simultaneously account for the scatter, size effects and temperature dependence of fracture toughness, as schematically presented in Fig. 11.12.

The method has been successfully applied to a very large number of different ferritic steels and it forms the basis of the ASTM testing standard for fracture toughness testing in the transition region [11.127]. Worldwide, there is ongoing comprehensive validation and development work to incorporate the Master Curve method, as a new reference fracture toughness concept, into different structural integrity assessment procedures including ASME Boiler and Pressure Vessel Code.

The Master Curve enables a complete characterization of a material's brittle fracture toughness based on only a few small-size specimens. The Master Curve method has been shown to be applicable for practically all steels with a body-centered cubic lattice structure, generally identified as ferritic steels.

The method enables the use of small specimens for quantitative fracture toughness estimation, thus reducing testing costs and enabling surveillance size specimens to be used for a direct measurement of fracture toughness. It also improves the quality of lower bound fracture toughness estimates, thus reducing the need for overly conservative safety factors. The applicability of the method is not restricted to nuclear applications. Its biggest impact is foreseen to be on fracture toughness determination for conventional structures, where testing costs and material use are presently inhibiting the use of fracture mechanics in design.

Recently, the Master Curve methodology has evolved from only being a brittle fracture testing and analysis procedure to a technological tool capable of addressing other important structural integrity issues such as constraint and transferability of fracture toughness characteristics.

11.6.2 Homogeneous Material

The approach is based on a statistical brittle fracture model, which gives for the scatter of fracture toughness provides a cumulative failure distribution in the following form:

$$P\left[K_{IC} \le K_I\right] = 1 - \exp\left(-\left[\frac{K_I - K_{min}}{K_0 - K_{min}}\right]^4\right) \qquad (11.20)$$

In Eq. (11.20), $P(K_{IC} \le K_I)$ is the cumulative failure probability, K_I is the stress intensity factor, K_{min} is the theoretical lower bound of fracture toughness and K_0 is a temperature and specimen size dependent normalization fracture toughness, that corresponds to a 63.2% cumulative failure probability being approximately 1.1 • (mean fracture toughness).

The Master Curve scatter expression is essentially a three-parameter Weibull distribution with two of the parameters fixed. As such, it has certain statistical characteristics presented as:

$$\bar{K}_I\text{-}K_{min}=(K_0\text{-}K_{min})\times\Gamma(1.25)=0.906\times(K_0\text{-}K_{min})$$

$$K_{0.5}\text{-}K_{min}=0.912\times(K_0\text{-}K_{min})$$

$$\sigma_{K_I\text{-}K_{min}}=(K_0\text{-}K_{min})\times\sqrt{\Gamma(1.5)\text{-}\Gamma(1.25)^2}=0.254\times(K_0\text{-}K_{min}) \qquad (11.21)$$

$$\sigma_{K_I\text{-}K_{min}}=(\bar{K}_I\text{-}K_{min})\times\sqrt{\frac{\Gamma(1.5)}{\Gamma(1.25)^2}\text{-}1}=0.281\times(\bar{K}_I\text{-}K_{min})$$

The most important information in Eq. (11.21) is that the mean and median toughness are essentially the same ($0.91\times[K_0\text{-}K_{min}]$) and that the characteristic scatter has a 28 % standard deviation with respect to the mean toughness.

The Master Curve scatter distribution can be expressed in a linear form using the form $0.25\{\ln[1/(1\text{-}P_f)]\}$. This produces a straight line starting with K_{min} and having a slope of $K_0\text{-}K_{min}$. This selection of coordinates is known as the Master Curve failure probability diagram. Experimentally, however, a straight line is seldom the result. This is due to the uncertainty connected to small data sets. As an example of the reliability of small sample data, Fig. 11.13 shows the reliability in terms of the Master Curve failure probability diagram coordinates. For data sets coming from distributions according to the straight line the Master Curve failure probability diagram, any results falling within the 5% & 95 % confidence bands is possible. It is clear from the figure that any attempt to estimate the Weibull slope or minimum value from small data sets is senseless. Even with a sample of 100, the estimate of the minimum value will have a considerable uncertainty. The only sensible approach is to fix all but one parameter.

The model predicts a statistical size effect of the form of Eq. (11.22)

$$K_{B_2}=K_{min}+\left[K_{B_1}-K_{min}\right]\cdot\left(\frac{B_1}{B_2}\right)^{1/4} \qquad (11.22)$$

where B_1 and B_2 correspond to respective specimen thickness (length of crack front).

On the lower shelf of fracture toughness (K_{IC} << $50\,MPa\sqrt{m}$) the equations may be inaccurate. The model is based upon the assumption that brittle fracture is primarily initiation controlled, even though it contains a conditional crack propagation criterion, which among others is the cause of the lower bound fracture toughness K_{min}, see e.g. [11.128]. On the lower shelf, the initiation criterion is no longer dominant, but the fracture is completely propagation controlled [11.128]. In this case there is no statistical size effect (Eq (11.22)) and also the toughness distribution differs (not very much) from Eq (11.20). In the transition region, where the use of small specimens becomes valuable, however, Eqs (11.20) and (11.22) are valid.

For structural steels, a "Master Curve" describing the temperature dependence of fracture toughness has been proposed by [11.129 and 11.130]. The temperature dependence, for a 25 mm thick specimen, has the form of Eq. (11.23).

$$K_0=31+77\cdot\exp\left(0.019\cdot\left[T-T_0\right]\right) \qquad (11.23)$$

T_0 is the transition temperature (°C) where the mean fracture toughness, is 100 $MPa\sqrt{m}$

Eq (11.23) gives an approximate temperature dependence of the fracture toughness for ferritic structural steels and it is comparatively well verified. The term ferritic includes also quenched and tempered martensitic and bainitic

structural steels. Keeping the temperature dependence fixed, decreases the effect of possible invalid fracture toughness values upon the transition temperature T_0. The temperature dependence does not work for precipitation hardened steels like maraging steels and it may also break down for steels where the failure occurs by grain boundary fracture.

Usually the separate test data are analysed directly by a combination of Eqs. (11.20), (11.22) and (11.23). This is possible when all specimens fail by brittle fracture. The analysis of data sets which include results ending in non-failure, is slightly more complicated. If some of the non-failure values are lower than some of the failure values, the data set is defined as being randomly censored. Moskovic, [11.131] has presented a general method of analysing randomly censored fracture toughness data sets. His method, based upon the maximum likelihood concept, is somewhat simplified when it is combined with Eqs (11.20), (11.22) and (11.23).

The maximum likelihood estimate, for a randomly censored data set, for estimating T_0 when the scatter obeys Eq (11.20) and the temperature dependence obeys the Master Curve (Eq (11.23)), gets the form of Eq. (11.24), where the units are in $MPa\sqrt{m}$ and Celsius.

$$\sum_{i=1}^{n} \frac{\delta_i \cdot \exp\{0.019 \cdot [T_i - T_0]\}}{11 + 77 \cdot \exp\{0.019 \cdot [T_i - T_0]\}} = \sum_{i=1}^{n} \frac{\left(K_{IC_i} - 20\right)^4 \cdot \exp\{0.019 \cdot [T_i - T_0]\}}{\left(11 + 77 \cdot \exp\{0.019 \cdot [T_i - T_0]\}\right)^5} \tag{11.24}$$

From Eq. (11.24), T_0 can be solved iteratively. The parameter delta (δ_i) is one (1) when K_{IC} corresponds to failure by brittle fracture and δ_i = 0 when K_{IC} corresponds to non-failure (end of test value).

When Eq. (11.24) is used to determine T_0, and the test temperatures are in the range $T_0 - 50^oC$ ... $T_0 + 50^oC$, the standard deviation of the estimate is approximately $\sigma_{T_0} \approx 17/\sqrt{r}$ °C, where r is total number of valid specimens used to establish T_0.

11.6.3 Inhomogeneous Material

Section 5.4.5.1 describes the procedure developed for the analysis of fracture toughness data, when the number of fracture toughness test results is limited and there is no prior knowledge regarding the materials homogeneity. The procedure contains three steps. Step 1 gives an estimate of the median value of fracture toughness. Step 2 performs a lower tail MML estimation, checking and correcting any undue influence of excessive values in the upper tail of the distribution. Step 3 performs a minimum fracture toughness value estimation to check and make allowance for gross inhomogeneities in the material. In Step 3, effectively, an additional safety factor is incorporated for cases where the number of tests is small.

Another method for the analysis of inhomogeneous fracture toughness datasets is given in Section 12. 4.

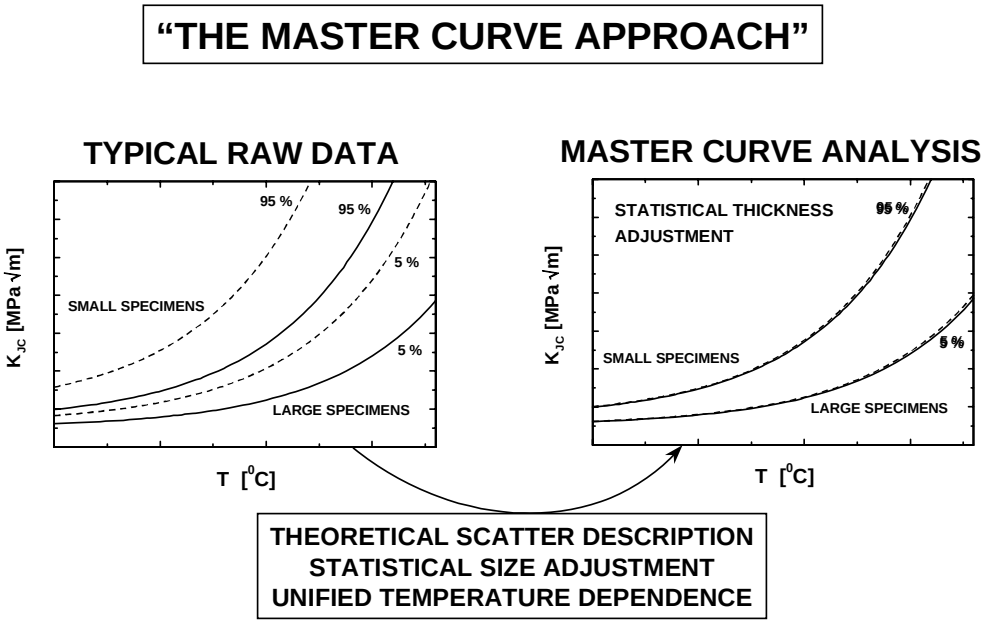

Figure 11.12 – Basic principle of the Master Curve method

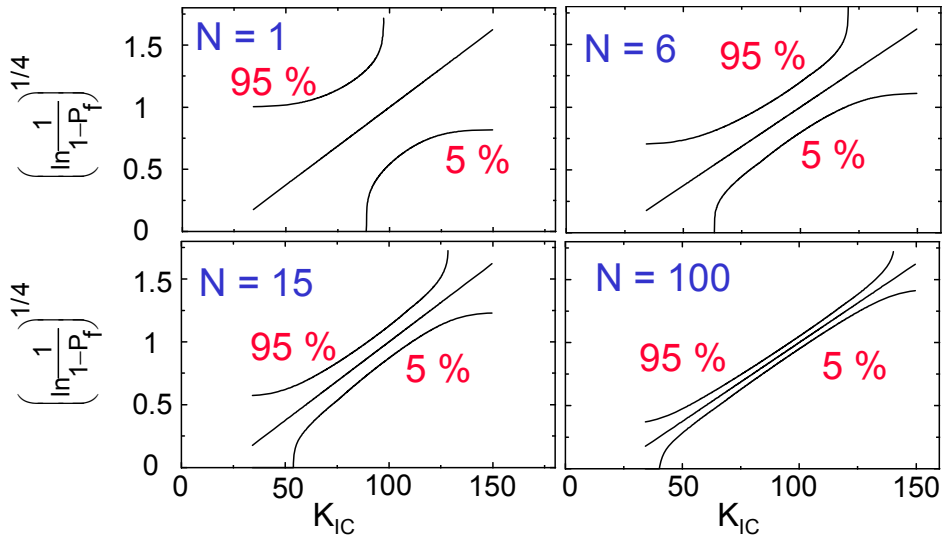

Figure 11.13 – Example of uncertainty related to small data sets

11.6.4 Bibliography

[11.126] Wallin, K. 1999. The master curve method: a new concept for brittle fracture. Int. J. of Materials and Product Technology. 14, 2/3/4, 342 – 354

[11.127] ASTM E1921-05 ‘Standard test method for determination of reference temperature, T0, for ferritic steels in the transition range’, February 2005

[11.128] Merkle, J. G., Wallin, K. and McCabe, D. E. 1998. Technical Basis for an ASTM Standard on Determining the Reference Temperature, T0, for Ferritic Steels in the Transition Range. NUREG/CR-5504, Oak Ridge National Laboratory, Oak Ridge

[11.129] Wallin, K. 1991. Fracture Toughness Transition Curve Shape for Ferritic Structural Steels. In: Fracture of Engineering Materials & Structures (eds. S. T. Teoh and K. H. Lee), p. 83. Elsevier Applied Science, London

[11.130] Wallin, K. 1993. Irradiation damage effects on the fracture toughness transition curve shape for reactor pressure vessel steels. Int J Pres Ves Piping 55, 61-79.

[11.131] Moscowic, R. 1993. Statistical analysis of censored fracture toughness data in the ductile to brittle transition temperature region. Engng Fracture Mech 44, 21-41.